Feng *et al. Chem Synth* 2024;4:43
DOI: 10.20517/cs.2024.12

Chemical Synthesis

Review

Open Access

Solid-state NMR of active sites in TiO_2 photocatalysis: a critical review

Ningdong Feng[1,2], Jun Xu[1,2,*], Feng Deng[1,2,*]

[1]National Center for Magnetic Resonance in Wuhan, State Key Laboratory of Magnetic Resonance and Atomic and Molecular Physics, Innovation Academy for Precision Measurement Science and Technology, Chinese Academy of Sciences, Wuhan 430071, Hubei, China.
[2]University of Chinese Academy of Sciences, Beijing 100049, China.

[*]**Correspondence to:** Prof. Jun Xu, Prof. Feng Deng, National Center for Magnetic Resonance in Wuhan, State Key Laboratory of Magnetic Resonance and Atomic and Molecular Physics, Innovation Academy for Precision Measurement Science and Technology, Chinese Academy of Sciences, No. 30, Xiaohongshan West District, Wuhan 430071, Hubei, China. E-mail: xujun@wipm.ac.cn; dengf@wipm.ac.cn

How to cite this article: Feng N, Xu J, Deng F. Solid-state NMR of active sites in TiO_2 photocatalysis: a critical review. *Chem Synth* 2024;4:43. https://dx.doi.org/10.20517/cs.2024.12

Received: 30 Jan 2024 **First Decision:** 11 Jun 2024 **Revised:** 13 Jun 2024 **Accepted:** 27 Jun 2024 **Published:** 5 Aug 2024

Academic Editor: Yann Garcia **Copy Editor:** Pei-Yun Wang **Production Editor:** Pei-Yun Wang

Abstract

Titanium dioxide (TiO_2) is one of the optimal semiconductor metal oxide photocatalysts with a wide range of application fields, such as heterogeneous catalysis, energy science, and environmental science. Solid-state nuclear magnetic resonance (NMR) spectroscopy is a powerful tool for characterizing both structure and dynamics at an atomic-molecular level in heterogeneous catalysts. In this review, we first provide a brief discussion on the progress in investigating the structures of titanium and oxygen in bulk and on the surface of TiO_2 by using various solid-state NMR techniques. Advances in the understanding of electronic structure and properties of TiO_2 with distinct surface features, including various crystal facets and heteroatomic adsorption by chemical probe-assisted NMR techniques, are secondly presented. The solid-state NMR characterization of heteroatom active sites (such as ^{13}C, ^{15}N, ^{11}B, ^{27}Al) and their function in TiO_2 photocatalysts is described in detail. Finally, a critical discourse assesses the current limitations and prospects of solid-state NMR in its application to the optimization and design of advanced TiO_2 photocatalysts.

Keywords: Characterization, solid-state NMR, TiO_2, photocatalyst, active sites

INTRODUCTION

Titanium dioxide (TiO_2) has emerged as a leading candidate in the field of photocatalysis owing to its unique confluence of desirable attributes: exceptional optical and electronic properties, robust thermal and chemical stability, environmental benignity, and economic viability. This advantageous combination has propelled TiO_2 to the forefront of research in diverse applications, including solar energy harvesting[1-3], photocatalytic hydrogen generation[4-6], CO_2 conversion[7-9], and organic pollutant degradation[10,11]. Since 2000, the statistical analysis reported that publications on TiO_2 photocatalysis crossed 10,000 per year, suggesting that this field has been intensively interested in research and development.

TiO_2 exists in three crystalline phases: anatase, rutile, and brookite, and the former two can be used as semiconductor photocatalysts. The structure of both rutile and anatase TiO_2 consists of chains of [TiO_6] units, where six O^{2-} ions surround one Ti^{4+} ion to form an octahedron[12]. However, due to the differences of each [TiO_6] octahedron distortion, the Ti–Ti and Ti–O distances, octahedron chain assemblies, the energy band structure and mass density between two crystalline phases of TiO_2 are different. Besides the crystalline phases, the differences in crystallite size and specific surface area, crystalline plane and morphology also cause change of properties in TiO_2 due to the subsequent change in structures and content of microscopic Ti and O sites on TiO_2 surface. For example, using K-edge X-ray absorption near edge structure (XANES) techniques, Chen *et al.* found that compared to the octahedron Ti sites in TiO_2 with big size (50 nm), severe distortion of the Ti site environment exists in TiO_2 nanoparticles with small size (1.9 nm)[13]. Due to the truncation of the lattice, the distorted Ti sites should be a penta-coordinate square pyramidal geometry, located mainly on the nanoparticle surface, responsible for the chemisorption of organic molecules. It was also found that more distorted bond angles of bridging oxygens (O–Ti_2) and more unsaturated Ti sites (pentacoordinated Ti^{4+}) are present on the (001) facet compared to the (101) facet[14,15]. All that lead to more active bridging O centers, easier O_2 adsorption, and higher surface energy on the (001) facet[16,17]. Yu *et al.* reported that the higher photocatalytic ability of TiO_2 thinner films was due to lesser opacity and more surface active sites[18]. Therefore, these microscopic active sites on the TiO_2 surface should play a crucial role in improving photocatalytic activities.

The semiconductors-based photocatalytic reactions should involve three steps [Figure 1][6,12,19-21]: Firstly, the electron-hole pairs (carriers) are excited by photons with an energy more than the band gap of TiO_2. Secondly, the photogenerated carriers separate or recombine during migration. Finally, the photogenerated carriers react with surface-adsorbed molecules through active sites on the TiO_2 surface. As well known, owing to the wide band gap (rutile of 3.0 eV, and anatase of 3.2 eV), ultraviolet (UV) radiation is a prerequisite to facilitating the formation of the carriers during the photocatalytic reaction. Since ca. 50% of the solar radiation on earth is in the visible (vis) region, UV light makes up only ca. 5% of the natural light spectrum; improving the absorption of solar light by TiO_2 has become one of the most urgent tasks in photocatalytic research and development. To solve this problem, some common and promising modification approaches, such as heteroatoms (ions) doping[1,22-32] and loading[1,19,32-41], have been utilized to narrow the band gap and enhance the separation efficiency of photogenerated carriers. Additionally, the reaction of photogenerated carriers on the TiO_2 surface is also crucial in photocatalysis, in which the photogenerated carrier transfers to surface active sites to form active intermediates, and then the active intermediates react with surface molecules[42-48]. For example, surface hydroxyl (OH)/oxygen (O) sites and adsorbed H_2O on TiO_2 can trap photogenerated holes to form active paramagnetic intermediates (such as $^{\bullet}$OH and Ti–O$^{\bullet}$)[43,44,49,50].

An in-depth understanding of active centers, including heteroatoms (ions) and surface active sites is the key to establishing structure-activity relationships, which can facilitate the rational design of highly efficient

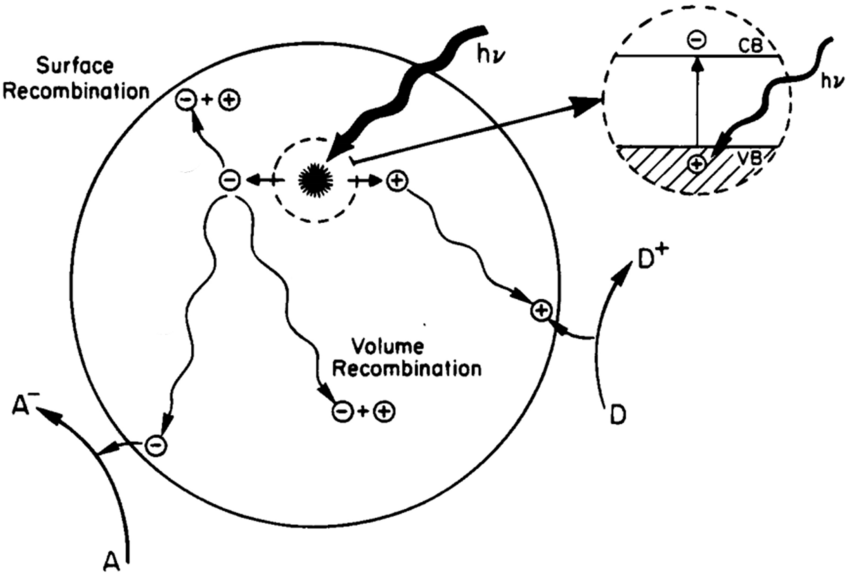

Figure 1. Semiconductors-based photocatalytic mechanism. Reproduced with permission from[12]. Copyright 1995, American Chemical Society.

TiO_2 photocatalysts. Thus, numerous techniques, such as high-resolution transmission electron microscopy (HRTEM), Raman spectroscopy, X-ray diffraction (XRD), X-ray photoelectron spectroscopy (XPS), Infrared (IR) spectroscopy, Electron paramagnetic resonance (EPR), solid-state nuclear magnetic resonance spectroscopy (NMR), *etc.*, have been employed to study the structure of photocatalysts and the relevant reaction mechanisms. Generally, the crystal structure is determined by HRTEM, XRD, and Raman spectroscopy[51-56], and the electronic structures can be studied by X-ray photoelectron and X-ray absorption and emission spectroscopies[57-60]. EPR has been used to detect defect sites [Ti^{3+} and oxygen vacancy (V_o)], and surface paramagnetic species ($O_2^{\bullet-}$, O^- species, and $^{\bullet}OH$)[42,50,61], while IR spectroscopy has been used to detect surface OH and reaction intermediates of EPR and NMR silence[17,53,62].

Among them, solid-state NMR is a powerful tool for characterizing the structure of solid-state materials at the atomic-molecular level[63-70]. Although research on solid-state NMR techniques for photocatalyst active-site structures and photocatalytic reactions is rapidly increasing [Figure 2], the research interest in the application of solid-state NMR techniques is still relatively low compared to other techniques in the field of photocatalysis. To the best of our knowledge, this article presents the first examination of the application of solid-state NMR to TiO_2 photocatalysis. Specifically, we conduct an overview of the advances made utilizing solid-state NMR techniques to analyze TiO_2 photocatalysts. Through selected examples from the literature, we demonstrate how solid-state NMR has been utilized to reveal the atomic structures and interactions between various sites or components within TiO_2. The review also discusses both the current limitations of solid-state NMR methodology in photocatalyst research and promising future directions for this technique.

TITANIUM AND OXYGEN ACTIVE SITES IN TIO_2

The past few decades have witnessed a surge in efforts dedicated to unraveling the structural and electronic intricacies of TiO_2, employing both experimental and theoretical approaches. However, the structure and coordination environments of Ti and O sites on the TiO_2 surface are very different from those in bulk and thus remain poorly understood due to the complex surface structures. A wide variety of active sites exist on the TiO_2 surface, including distorted Ti sites, low-coordinated Ti sites, bridging O sites, tri-coordinated O

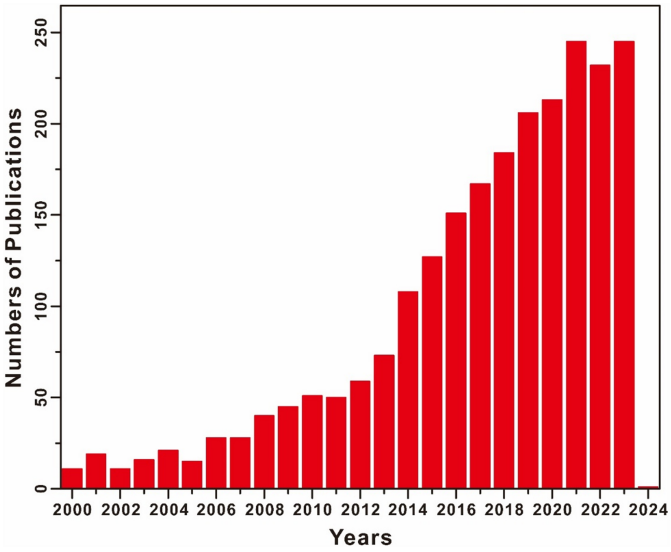

Figure 2. Yearly number of publications and stepwise development for photocatalysts studied by NMR spectroscopy. NMR: Nuclear magnetic resonance.

sites, *etc.* The distorted Ti sites, such as the double-bonded titanyl (Ti=O) groups on the (011) surface of reconstructed rutile TiO_2, can promote the dissociation of part of adsorbed water[71,72]. The coordinatively unsaturated Ti atoms, including the penta-coordinated Ti sites (TiO_5) on the surface and the tetra-coordinated Ti sites (TiO_4) on the edge/corner, are important anchoring sites for the adsorption of targeted molecules (such as H_2O, HCHO, and ethylene)[73-76] and for maintaining the high stability of the cocatalysts (such as Pd, Ru, Au, *etc.*)[77-79]. Theoretical calculations predicted that the bridging O sites (OTi_2) of TiO_2 can interact with the proton and facilitate the dissociation of H_2O, which are closely related to catalytic mechanisms[80-82]. Furthermore, the coordinatively unsaturated Ti and O sites serve as active sites for charge carrier trapping and molecular adsorption during CO_2 reduction and methanol conversion[83-85]. Thus, determining the structure and distribution of the Ti and O sites on TiO_2 is a prerequisite for understanding the structure-property relationship.

Titanium active sites in TiO_2

$^{47/49}$Ti NMR can be utilized to detect the local environments of Ti sites in TiO_2 photocatalysts[86-88]. However, the isotopes have a low natural abundance, with ^{47}Ti at 7.28% and ^{49}Ti at 5.51%. They also exhibit low Larmor frequencies, measuring 22.55 MHz at a magnetic field of 9.4 T. Additionally, the Ti atoms in TiO_2 photocatalysts are quadrupole nuclei, with spin quantum numbers of I = 5/2 for ^{47}Ti and I = 7/2 for ^{49}Ti. These nuclei possess a relatively low gyromagnetic ratio and experience significant quadrupolar interactions, which lead to low sensitivity and resolution of these spectra due to the wide signal lineshape[89-91]. The $^{47/49}$Ti static NMR spectra were used to monitor the transition of the crystalline phases of brookite, anatase, and rutile in as prepared TiO_2 at different annealing temperatures from 400 to 850 °C, and $^{47/49}$Ti NMR parameters were extracted from the spectral simulations of the corresponding components of bulk polycrystalline phases [Figure 3][92,93]. The size, crystallinity, and crystal phase of TiO_2 can sensitively be reflected on the lineshape of the corresponding NMR signal. For example, the ^{49}Ti NMR parameters, including chemical shift (δ_{iso}), quadrupole coupling constant (C_Q), and asymmetry parameter (η), for anatase were determined to be -67 ppm, 4.6 MHz, and 0.1, respectively, whereas for rutile the corresponding ^{49}Ti NMR parameters are -15 ppm, 13.4 MHz, and 0.2, respectively. It was found that the narrow peak should be the ^{49}Ti NMR signal in TiO_2 bulk and the other relatively broad peak should be the ^{47}Ti NMR signal in TiO_2 bulk. With the increase of annealing temperature to 700 °C, the quadrupole linear patterns of ^{47}Ti and ^{49}Ti

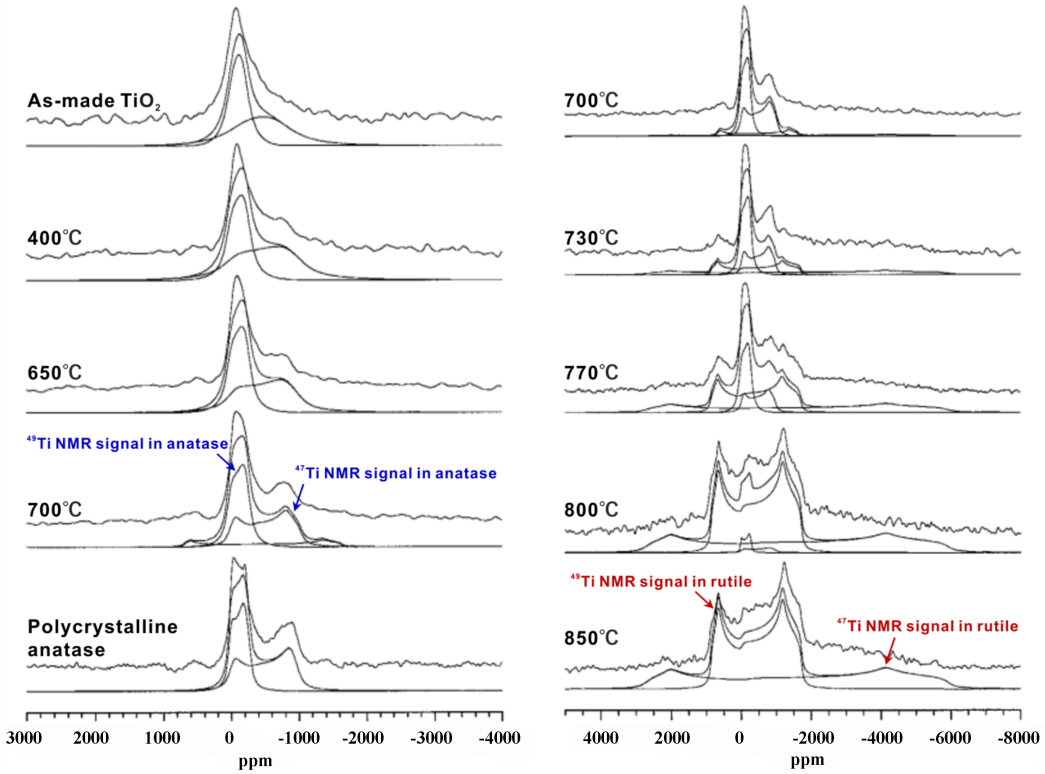

Figure 3. Experimental and simulated static Hahn-echo $^{47/49}$Ti NMR spectra of TiO_2. The TiO_2 nanoparticles were annealed before solid-state NMR experiments at variable temperatures. Reproduced with permission from[93]. Copyright 2001, American Chemical Society. NMR: Nuclear magnetic resonance.

static NMR signals become more pronounced, indicating that the crystallinity of the anatase becomes better. With the further increase of annealing temperature, two NMR signals corresponding to ^{47}Ti and ^{49}Ti in rutile bulk increase gradually at the expense of the ^{47}Ti and ^{49}Ti NMR signals in anatase bulk, indicating the transition of crystal phase from anatase to rutile.

However, a long-time (ca. 20 h) acquisition at 33.81 MHz using a CMX Infinity 600 spectrometer and large sample quantity (9.5 mm rotor) was necessary to ensure the signal-to-noise ratio of the spectra, and it is difficult to differentiate and assign the seriously overlapped resonances due to the large chemical shift anisotropy (CSA) and quadrupolar interactions. The advanced NMR techniques have been developed to optimize the signal excitation and acquisition. Bräuniger *et al.* use fast amplitude-modulated (FAM) radiofrequency (RF) pulse trains to enhance the sensitivity of the signal via transferring spin population from the satellite transitions to central transition[94]. In comparison with Hahn-echo acquisition, the intensity of the $^{47/49}$Ti central-transition line has increased by more than twice in the magic angle spinning (MAS) NMR spectra of TiO_2.

As well known, the ^{47}Ti and ^{49}Ti isotopes exhibit almost identical Larmor frequencies and natural abundances[89]. Thus, to analyze the Ti sites of TiO_2, it is important to distinguish the ^{47}Ti and ^{49}Ti signals in the NMR spectra. When these isotopes occur in sites with a significant electric field gradient (EFG), the different nuclear spin quantum numbers would result in varying effective RF fields for the central transition nutation frequencies. As such, Larson *et al.* proposed isotope-selective quadrupolar Carr-Purcell Meiboom-Gill (QCPMG) pulse sequence to selectively excite the ^{47}Ti or ^{49}Ti powder linear[95]. The authors performed

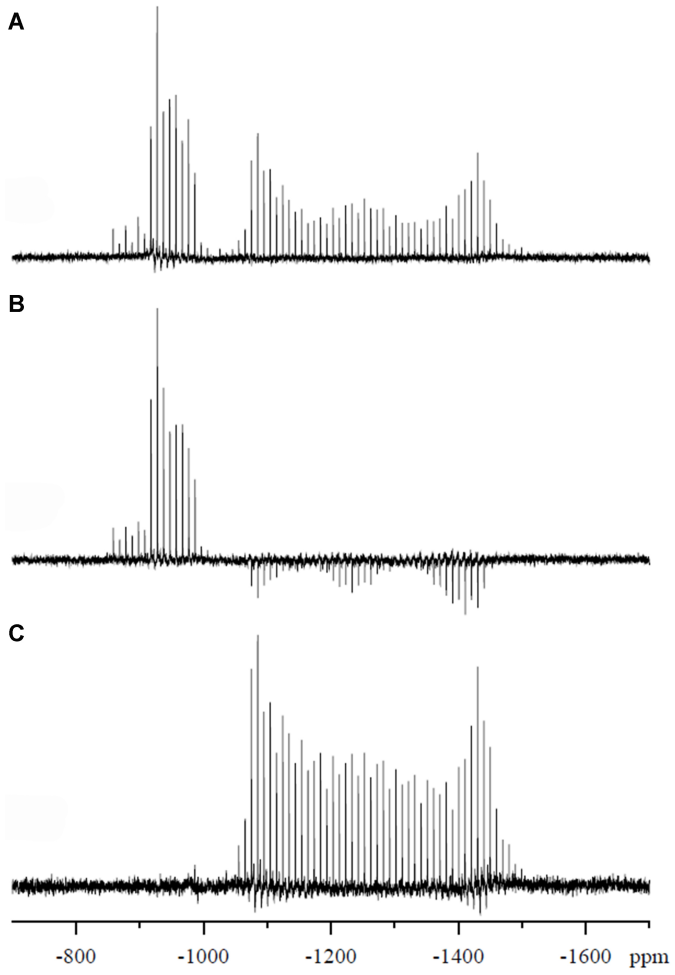

Figure 4. Experimental static ^{47}Ti and ^{49}Ti NMR spectra of anatase using the QCPMG pulse sequence. (A) The ordinary QCPMG pulse sequence; (B) the devised ^{49}Ti-selective pulse sequence; and (C) the devised ^{47}Ti selective pulse sequence. Reproduced with permission from[95]. Copyright 2006, Elsevier. NMR: Nuclear magnetic resonance; QCPMG: quadrupolar Carr-Purcell Meiboom-Gill.

solid-state NMR experiments and numerical simulations on the anatase and rutile of TiO_2. The ^{47}Ti and ^{49}Ti isotopes for anatase, with different quadrupolar interaction between the EFG at the titanium site and their nuclear quadrupole moments (Q), were separated at the field of 21.1 T, and their EFG and CSA tensors were accurately determined [Figure 4].

Precisely discerning the diverse Ti environments in TiO_2 presents a significant analytical challenge in static $^{47/49}$Ti NMR due to the significant overlap and inherent broadness of their spectral signatures. To overcome this problem, Epifani *et al.* used the MAS method at 12 kHz. This approach effectively improved the resolution of their NMR signals, allowing for a more detailed and accurate characterization of the titanium environments in both pristine TiO_2 and V_2O_5-loaded TiO_2 samples[96]. As shown in Figure 5, two resonances at 213 and -245 ppm were present in the $^{47/49}$Ti MAS NMR spectrum of amorphous TiO_2 before high-temperature heating (Figure 5, Left), which correspond to surface Ti bonded to OH and lattice Ti sites in TiO_2, respectively. A new dominant ^{49}Ti resonance at 792 ppm appeared after heating at 400-500 °C. The resonance at 792 ppm was even more intense in the $^{47/49}$Ti MAS NMR spectrum of TiO_2-V_2O_5 nanocrystals (Figure 5, Right). The new signal of 792 ppm should be ascribed to surface Ti sites, having a unique distorted tetrahedral environment unlike that of bulk anatase TiO_2. The V_2O_5 loading facilitates the

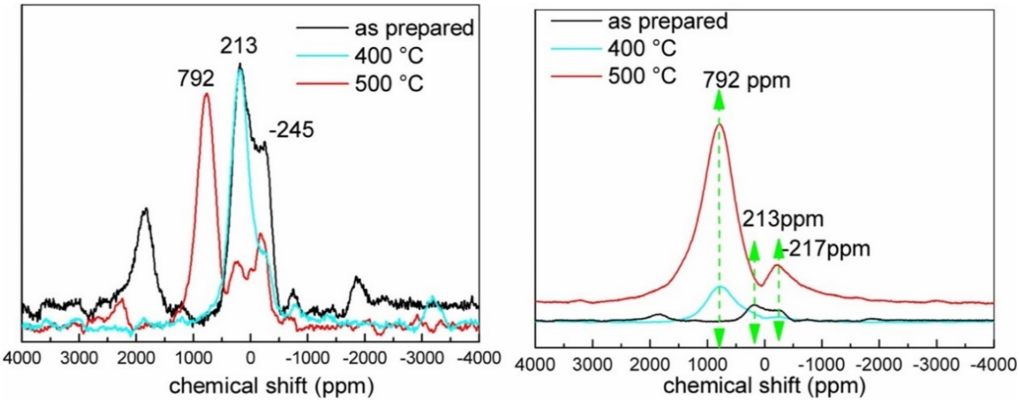

Figure 5. $^{47/49}$Ti MAS NMR spectra. (Left) pristine TiO_2 samples are examined as prepared, and after heating at 400 and 500 °C. (Right) V_2O_5-loaded TiO_2 samples were examined under identical conditions. Reproduced with permission from[96]. Copyright 2015, Elsevier. MAS: Magic angle spinning; NMR: nuclear magnetic resonance.

rearrangement of surface Ti sites to distorted tetrahedral geometry.

Oxygen active sites in TiO_2

Oxygen is another most important constituent atom of TiO_2 and plays a critical role in various chemical processes that occur on the catalyst surface. Thus, an understanding of the structure and distribution of the O sites helps develop more efficient and effective catalytic systems for energy storage and conversion. As previously reported[67-70,97-102], ^{17}O MAS NMR can be utilized to distinguish the local structures of oxygen sites in oxygen-containing materials. However, the ^{17}O quadrupolar nucleus (I = 5/2) exhibits a relatively low gyromagnetic ratio (γ = -5.774 MHz·T^{-1}) and low ^{17}O abundance (0.037%). Thus, it is difficult to use ^{17}O NMR to study the oxygen-containing materials in conventional magnetic fields (≤ 14.1 T), and the ^{17}O isotopic entailment is necessary to acquire the ^{17}O MAS NMR spectra[103]. In the earlier study, the ^{17}O enriched TiO_2 was commonly prepared by hydrolysis of organic titanate [such as Ti(Oi-Pr)$_4$] using ^{17}O enriched H_2O[101] or high-temperature calcination of TiO_2 using ^{17}O enriched O_2[104]. Accordingly, the ^{17}O NMR signal of bulk oxygen, which is predominant in TiO_2, was solely observed. The ^{17}O MAS NMR spectrum of anatase and rutile TiO_2 exhibits a single resonance at 562 and 596 ppm, respectively, which was assigned to tri-coordinated oxygen (OTi_3) in the corresponding crystal phase. Besides the resonance in the anatase (562 ppm) or rutile (596 ppm) domain, three resonances at 516, 543, and 572 ppm, corresponding to distorted OTi_3 or tetra-coordinated oxygen (OTi_4) sites on the interface between anatase and rutile, were observed in the spectra of mixed-phase TiO_2 [Figure 6].

Recently, Li *et al.* used 90% ^{17}O-enriched H_2O to realize surface-selectively ^{17}O-labeled anatase TiO_2 with dominant exposed (001) facets [TiO_2(001)] and anatase TiO_2 with dominant exposed (001) facets [TiO_2 (101)] [Figure 7][105]. Based on the ^{17}O MAS NMR spectra and theoretical calculations, surface O sites on TiO_2 exposing different facets were roughly distinguished. The signals at high frequencies (600-780 ppm) can be attributed to bridging O sites (OTi_2); the peaks at 460-580 ppm should be due to tri-coordinated oxygen (OTi_3) species; the resonances at lower frequencies (100-250 ppm) can be assigned to hydroxyl groups (Ti–OH); the signals at -200-30 ppm can be ascribed to adsorbed H_2O. The ^{17}O NMR parameters, including quadrupole coupling constant (C_Q) and asymmetry parameter (η) [Table 1]. In addition, it has been accepted that the type, content, and structure of oxygen sites on different crystal surfaces vary greatly due to the difference in surface defects and reconstruction, which can be studied by ^{17}O MAS NMR spectroscopy. The ^{1}H → ^{17}O cross-polarization (CP) MAS and two-dimensional (2D) heteronuclear correlation (HETCOR) NMR have been utilized to probe the spatial proximity of the H and O atoms,

Table 1. Summary of the ^{17}O MAS NMR signals occurring in the spectra of TiO_2, their chemical shifts (δ_{iso}), quadrupole coupling constants (C_Q), asymmetry parameters (η), and assignments according to literature

δ_{iso} (ppm)	C_Q (MHz)	η	Assignment	Ref.
600-750	< 1.7	0.3-0.8	OTi_2 on anatase surface	[105]
535-570	1.1-1.5	0.2-0.8	OTi_3 in anatase	[105]
530-550	ca. 1.0	0.5-1.0	OTi_3 on anatase (001) facet	[105]
500-560	1.1-1.7	0.5-0.8	OTi_3 on anatase (101) facet	[105]
572	2.0	0.1	OTi_3 in low-ordered TiO_2	[104]
596	1.8	0.6	OTi_3 in rutile	[104]
543	1.6	0.6	Distorted OTi_3 or OTi_4 near interface between anatase and rutile	[104]
516	1.8	0.8	Distorted OTi_3 or OTi_4 near interface between anatase and rutile	[104]
100-300	6.2-7.0	0.1-0.5	OH on anatase surface	[105]
21	8.37	0.71	H_2O absorbed at step-edge Ti_{5C} OA	[105]
7	8.58	0.7	H_2O absorbed at step-edge Ti_{5C} OB	[105]

MAS: Magic angle spinning; NMR: nuclear magnetic resonance; OA: orientation A; OB: orientation B.

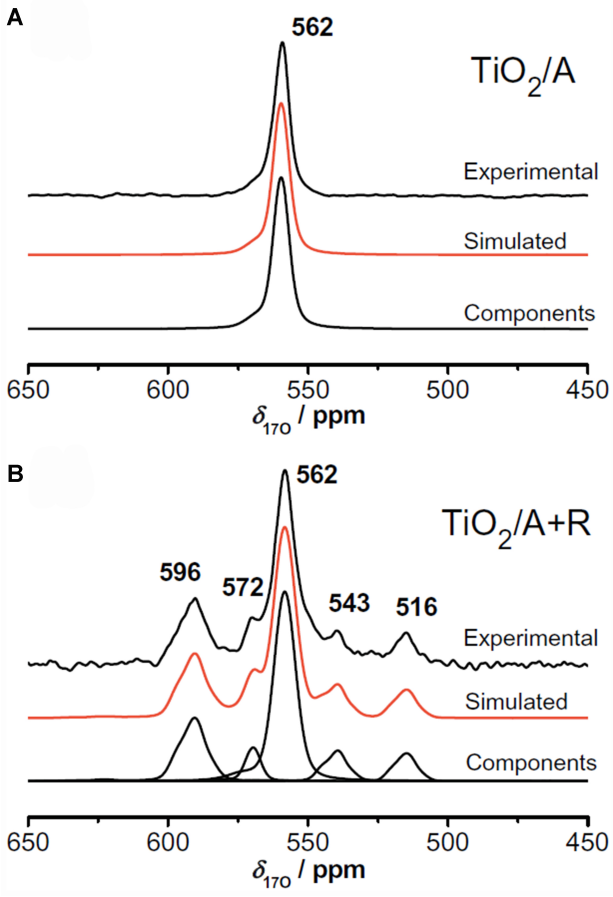

Figure 6. ^{17}O MAS NMR spectra of anatase TiO_2 and mixed-phase TiO_2 of anatase and rutile with ^{17}O enrichment. Reproduced with permission from[104]. Copyright 2014, Elsevier. MAS: Magic angle spinning; NMR: nuclear magnetic resonance.

which, however, is time-consuming and exhibits low detection efficiency for the quadrupolar nucleus with low γ and low surface abundance[106-108]. These conventional correlation NMR techniques validated the

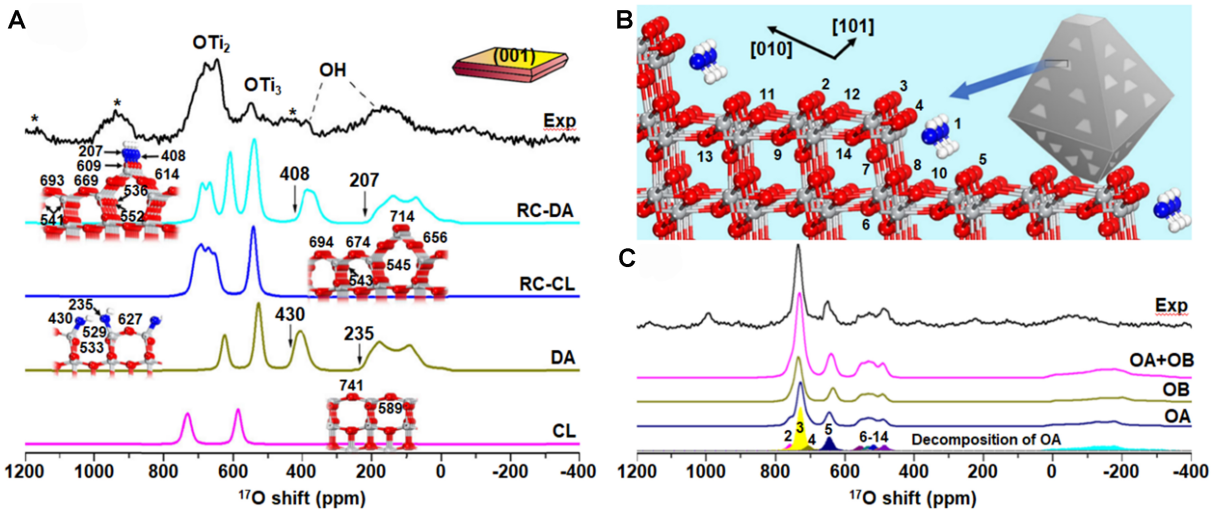

Figure 7. (A) Experimental and simulated 1D ^{17}O MAS NMR spectra of TiO_2 (001). The simulated spectra are based on DFT calculations on different structures; (B) The structure model of TiO_2 (101); (C) Experimental and simulated 1D ^{17}O MAS NMR spectra of the fully dried surface-selectively ^{17}O-labeled TiO_2 (101) (black line). The simulated spectra (colored lines and peaks) by using parameters obtained from DFT calculations. Reproduced with permission from[105]. Copyright 2017, Springer Nature. 1D: One-dimensional; MAS: magic angle spinning; NMR: nuclear magnetic resonance; DFT: density functional theory.

assignment of surface OH and adsorbed H_2O on the TiO_2 surface[106]. To date, it is a great challenge to identify the atomic-level structures of surface O species (including O sites, OH groups, and interfacial H_2O) and the detailed interactions between them on TiO_2 due to the complexity of the interfacial environments, the high mobility of interfacial H_2O, and the interference from outer-layer H_2O[109,110].

SURFACE TITANIUM AND OXYGEN SITES STUDIED BY SURFACE-ENHANCED NMR SPECTROSCOPY

Due to the high price of isotope reagents, low detection sensitivity, and low surface atomic content, it is difficult to acquire the $^{47/49}Ti$ and ^{17}O NMR spectra in a short time. Dynamic nuclear polarization (DNP) transfers the polarization of paramagnetic centers to nearby nuclei by microwave irradiation, which can enhance NMR signals in the ratio of the gyromagnetic ratio of the electron and the polarized nucleus. The DNP NMR spectroscopy instruments need to set up microwave sources and cryogenic probes ($T < 120$ K) to achieve efficient polarization transfer via cross effect, solid effect, and Overhauser effect[111-118]. The NMR signal enhancement techniques have been used to examine the surface structure of a variety of inorganic and hybrid materials[119-122], known as DNP-surface-enhanced NMR spectroscopy (SENS).

Direct DNP transfers polarization directly to target nuclei[123-125], and indirect DNP transfers polarization first to ^1H nuclei and then to target nuclei by CP[126-129]. Both of them can be realized for TiO_2 photocatalysts[130,131]. Chen *et al.* prepared ^{17}O-enriched TiO_2 by ball milling (BM) with ^{17}O-enriched H_2O at different times[130]. In the ^{17}O MAS NMR spectra [Figure 8A], the signals at around 560 ppm correspond to OTi_3 sites. Additionally, the underlying weaker resonances (at 500-600 ppm) corresponding to distorted/disordered OTi_3 sites and surface defects were also observable with the help of ultra-high field ^{17}O NMR [Figure 8B]. However, there was no clear evidence of surface Ti–OH groups (200 ppm) present. The ^{17}O DNP-SENS technique was utilized to detect the surface oxygen sites [Figure 8C and D]. In the direct-excitation ^{17}O DNP spectrum [Figure 8C], in addition to the intense signal of OTi_3 sites nearby the TiO_2 surface, another weak signal was observed at ca. 200 ppm, which can be assigned to a small amount of Ti–OH species. The surface Ti–OH species could be selectively detected using $^1H \rightarrow {}^{17}O$ DNP CP MAS NMR

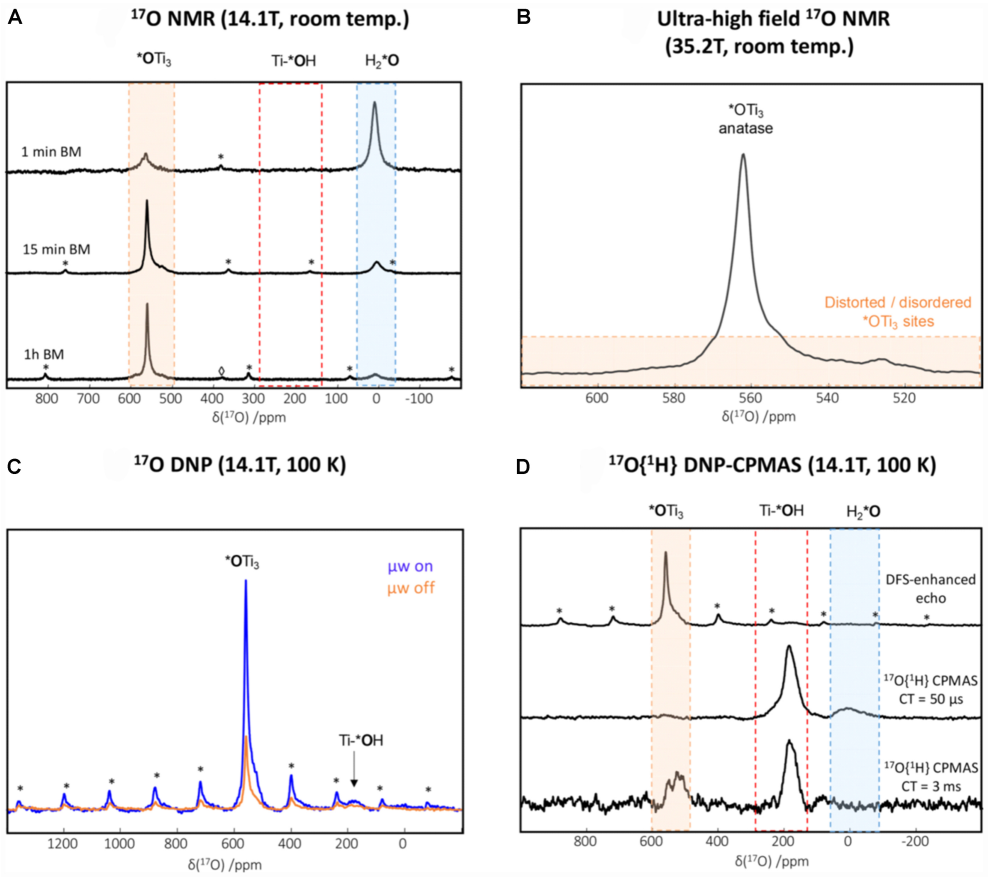

Figure 8. (A) ^{17}O MAS NMR spectra recorded at 14.1T on ^{17}O enriched TiO_2; (B) ^{17}O MAS NMR spectrum recorded at 35.2 T on a TiO_2 phase enriched in ^{17}O; (C) ^{17}O DNP NMR spectrum of a TiO_2 phase enriched in ^{17}O; (D) ^{17}O DNP CPMAS NMR spectra in comparison to the DFS-enhanced echo spectrum. Reproduced with permission from[130]. Copyright 2020, American Chemical Society. MAS: Magic angle spinning; NMR: nuclear magnetic resonance; DNP: dynamic nuclear polarization; CPMAS: cross-polarization magic angle spinning; DFS: double-frequency sweep.

experiments at a short contact time (50 μs, Figure 8D). With the increase of contact time (3 ms), the weak resonances of disordered/distorted OTi_3 sites could be observed as well, suggesting that these oxygen species were in close spatial proximity to protons.

The long-standing obstacle of acquiring well-resolved ^{17}O and/or $^{47/49}$Ti NMR spectra of TiO_2 photocatalysts at natural abundance has been overcome with the implementation of DNP techniques. To measure the surface O and Ti structures, Nagashima *et al.* developed a novel pulse sequence of refocused insensitive nuclei enhanced by polarization transfer (RINEPT)-$SR4_1^2$ (tt)-QCPMG [Figure 9A] capable of probing the local structure of half-integer spin quadrupolar nuclei[131]. Compared to CP, this novel method on the basis of the refocused insensitive nuclei enhanced by polarization transfer (INEPT) pulse sequence with adiabatic dipolar recoupling is more convenient for optimization and does not result in distorted quadrupolar line shapes. Accordingly, this technique has been used to probe the atomic-level structure of MoO_3-supported TiO_2 (MoO_3/TiO_2) photocatalyst.

The ^{1}H → $^{47/49}$Ti DNP-enhanced RINEPT-$SR4_1^2$ (tt)-QCPMG spectrum can observe selectively the signals of $^{47/49}$Ti species nearby the MoO_3/TiO_2 surface. Four signals were detected in the ^{1}H → $^{47/49}$Ti RINEPT-$SR4_1^2$ (tt) spectrum: ^{47}Ti of anatase TiO_2, ^{49}Ti of anatase TiO_2, ^{49}Ti of amorphous TiO_2, and ^{49}Ti surface signal

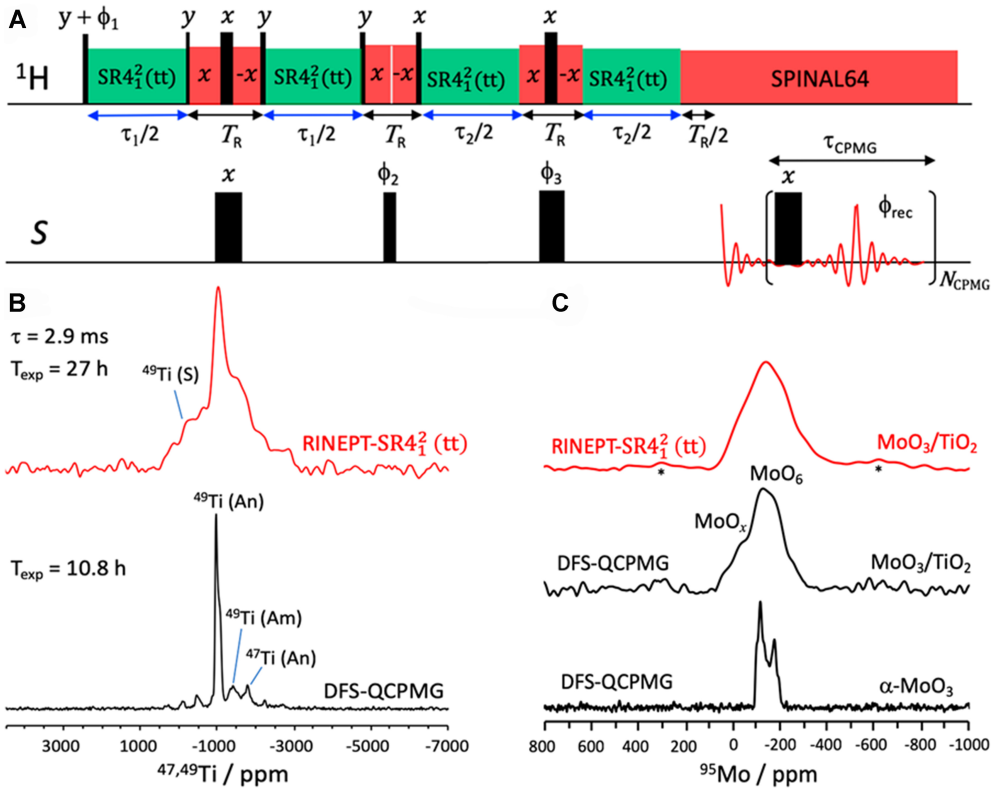

Figure 9. (A) Pulse sequence of RINEPT-$SR4_1^2$ (tt)-QCPMG used to transfer the DNP-enhanced ^1H polarization to the half-integer quadrupolar nucleus, S; (B) $^{47/49}Ti$ QCPMG NMR spectra of unmodified MoO_3/TiO_2 enhanced by indirect DNP using $^1H \rightarrow {}^{47/49}Ti$ RINEPT-$SR4_1^2$ (tt) transfer and DFS scheme; (C) ^{95}Mo QCPMG spectra enhanced by indirect DNP using $^1H \rightarrow {}^{95}Mo$ RINEPT-$SR4_1^2$ (tt) transfer of MoO_3/TiO_2 and by DFS of MoO_3/TiO_2 and α-MoO_3. Reproduced with permission from[131]. Copyright 2020, American Chemical Society. RINEPT: Refocused insensitive nuclei enhanced by polarization transfer; QCPMG: quadrupolar Carr-Purcell Meiboom-Gill; DNP: dynamic nuclear polarization; NMR: nuclear magnetic resonance; DFS: double-frequency sweep.

[^{49}Ti(S)] [Figure 9B]. The surface ^{49}Ti nuclei should be bonded to OH or OMo groups on MoO_3/TiO_2[131]. The same DNP-enhanced technique was used to detect the surface Mo species. In the $^1H \rightarrow {}^{95}Mo$ RINEPT-$SR4_1^2$ (tt) spectrum [Figure 9C], two kinds of Mo species, MoO_6 and MoO_x (x = 4, 5), were present on MoO_3/TiO_2. Comparing the double-frequency sweep (DFS)-QCPMG spectra of MoO_3/TiO_2 and α-MoO_3 [Figure 9], the ^{95}Mo signal of MoO_3/TiO_2 is much more broadened, indicating that there are more disordered structures near the surface and some ^{95}Mo nuclei are too far away from the protons on MoO_3/TiO_2.

The $^1H \rightarrow {}^{17}O$ RINEPT-$SR4_1^2$ (tt)-QCPMG experiments were performed at variable recoupling times to probe protonated and unprotonated oxygen species [Figure 10][131]. For a recoupling time (τ) of 1.9 ms, the RINEPT-$SR4_1^2$ (tt) can transfer the polarization from protons to ^{17}O nuclei. The indirect DNP technique based on RINEPT-$SR4_1^2$ (tt) can transfer the polarization from protons to ^{17}O nuclei with an estimate of the distance ca. 3.5 Å. Six ^{17}O signals were present in MoO_3/TiO_2, corresponding to OTi_3 sites (553 ppm) in the bulk of anatase, OTi_2 sites (650 ppm) on the surface of TiO_2, OMo_2 (420 ppm), OMo_3 (285 ppm), OMo_4 (150 ppm) and OMo_5 (20 ppm) sites of the supported MoO_3. For the recoupling time (τ) of 0.1 ms, the $^1H \rightarrow {}^{17}O$ RINEPT-$SR4_1^2$ (tt) experiment can selectively observe the protonated ^{17}O sites at the surface, which are at a distance of about 1 Å from the protons. Four ^{17}O signals were observable on the surface of MoO_3/TiO_2, including Ti–OH (130 ppm) of TiO_2, HOMo (-45 ppm), $HOMo_2$ (-266 ppm), and $HOMo_3$ (-390 ppm) of the supported MoO_3. Such detailed information on the various oxygen and titanium structures is expected

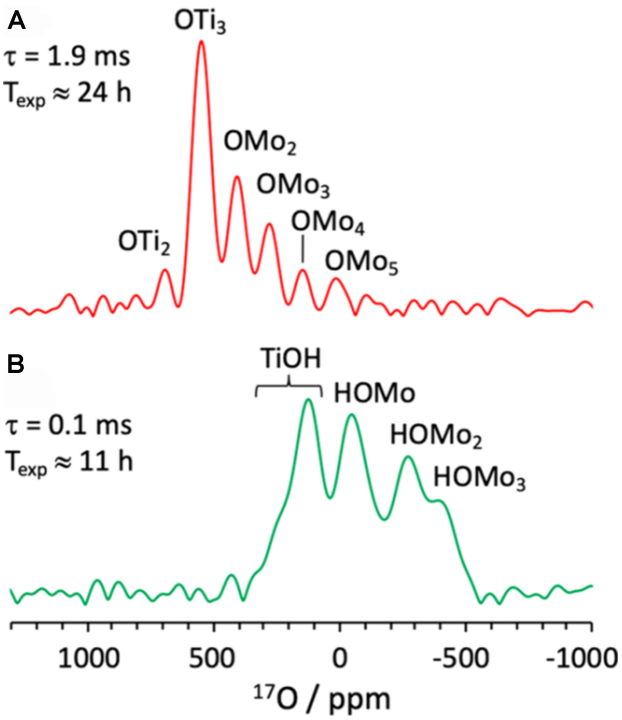

Figure 10. DNP-enhanced $^{1}H \rightarrow {}^{17}O$ RINEPT-SR4$^{2}_{1}$ (tt)-QCPMG spectra of unmodified MoO_3/TiO_2 with τ = (A) 1.9 and (B) 0.1 ms. Reproduced with permission from[131]. Copyright 2020, American Chemical Society. DNP: Dynamic nuclear polarization; RINEPT: refocused insensitive nuclei enhanced by polarization transfer; QCPMG: quadrupolar Carr-Purcell Meiboom-Gill.

to propose structure models of the anatase surface, which would facilitate the understanding of the structure-activity relationship.

The water adsorption and dissociation on the surface of metal oxide is a subject of immense importance in various fields such as photocatalysis, energy science, and material science[2,132-138]. This is because water plays a critical role in various chemical processes that occur on the surface of these materials[42,139-143]. A detailed understanding of the adsorption and dissociation of interfacial H_2O on these surfaces can help researchers develop more efficient and effective catalytic systems and materials for energy storage and conversion. It has been confirmed that a water molecule could react with the oxygen vacancy or rupture over the low coordination surface Ti sites of TiO_2, and form hydroxyls[141,144-147]. However, water adsorption and dissociation on nondefect titanium sites have been disputed for decades[82,148-152]. It is difficult to distinguish the Ti–OH groups formed by H_2O dissociation on nondefect TiO_2 surface from either the Ti–OH groups generated by H_2O reaction with defect sites or the original Ti–OH groups present on TiO_2. The DNP-SENS technique would provide the possibilities for exploring the detailed mechanism of water adsorption and dissociation on metal oxide.

SURFACE ELECTRONIC STRUCTURE AND PROPERTIES STUDIED BY PROBE-ASSISTED NMR TECHNIQUES

Surface structural features (including oxygen vacancies, cations, anions, and hydroxyl groups) play crucial roles in the development of efficient catalysts, especially metal oxides, and have been widely investigated[17,153-164]. The differences in these surface features result in the nano-sized particles with different physical/chemical properties. Taking anatase TiO_2 nanocrystallite as an example, each facet [including (101) and (001) facet] possesses distinctive chemical properties due to the differences in both the content and

electronic structure of the surface species from facet to facet. Probe molecules, including ^{13}C-carbon monoxide, ^{15}N-pyridine, and ^{31}P-trimethylphosphine (TMP), can be adsorbed onto catalysts, and their different NMR chemical shift values can reflect the various microenvironments of catalyst surfaces. Thus, the chemical probe-assisted NMR has been used to characterize the electronic structure in catalyst structures. Among them, TMP is a sensitive and reliable chemical probe to clarify qualitative and quantitative information on the adsorbed sites of the various catalysts[165-168]. In general, the ^{31}P chemical shift of -2~-5 ppm is ascribed to the TMP interacting with surface H^+ (Brönsted acid, BA site), while the ^{31}P chemical shift of -20~-58 ppm corresponds to the TMP interacting with surface exposed metal sites (i.e., Lewis acid, LA site), and a linear correlation between the ^{31}P chemical shift and the LA strength (or the binding energy) was found[169,170].

For TiO_2 nanoparticles, TMP, as the nucleophilic probe molecule, can strongly interact with the unsaturated coordinated Ti sites on the surface (that is, the surface TMP-Ti complex). Based on the ^{31}P chemical shift of the TMP-Ti complexes, surface Ti sites on various facets with different strengths of LA, surface energies, and spatial structure can be identified. Recently, Peng *et al.* prepared high-quality anatase TiO_2 nanocrystals with different exposed facets using hydrothermal synthesis with variable hydrogen fluoride (HF, 0-6 mL), labeled as TiO_2 powder with 90% (101) facet, (101)-dominated TiO_2 with 80% (101) facet, and (001)-dominated TiO_2 with 75% (001) facet [Figure 11A-C][162,164]. Probe-assisted ^{31}P solid-state NMR spectroscopy was employed to study the surface features and provided extraordinary sensitivity to their chemical states [Figure 11D-F]. There was almost no TMP-H^+ complex at -2~-5 ppm present on the TiO_2 powder but the TMP-LA complex had a main signal at -36 ppm and a small shoulder at -29 ppm. According to a previous report[171], the major peak and the shoulder with the integrated area ratios of 89.8% and 10.2% were attributed to the interaction between TMP and surface five-coordinate Ti sites (Ti_{5C}) on (101) and (001) facets, respectively, which is consistent with the density functional theory (DFT) calculation [Figure 11G and H]. When the TMP interacts with the Ti_{5C} sites on the reconstructed (1 × 4) (001) facet [$(001)_{RC}$], the chemical shift of ^{31}P NMR should be 50 ppm [Figure 11I]. Thus, the TMP-assisted NMR experiment can differentiate between facets of decreasing energy through their chemical shift values: (001) > (101) > $(001)_{RC}$ [Figure 11G-I]. Noteworthily, F ions are retained on the (101) and (001) facets when the TiO_2 samples were prepared with HF. Owing to the electronic withdrawing effect of surface F ions exerted on Ti_{5C} on these two facets, around 5-7 ppm downshift in chemical shift of the (101) and (001)-dominated TiO_2 retained F ions from the corresponding facets of -36 ppm (101) and -29 ppm (001) in the powder sample to -31 and -22.5 ppm, respectively. The NMR signal of -42.5 ppm was ascribed to the formation of F-containing surface oxygen vacancies on unstable (001) facets. Additionally, the significant increase of the Brønsted acid signal (-2~-3 ppm) was rationalized by the interaction of protons with the fluorine (F). The surface F on the (001) and (101) facets significantly enhanced the LA strength of Ti_{5C} sites by reflecting a downshift of ^{31}P chemical shift. On the other hand, the post calcination of the prepared TiO_2 led to partially replacing F with OH, rendering an upshift of ^{31}P chemical shift, suggesting the LA strength of Ti_{5C} decreased. The TiO_2 surfaces tend to adsorb various surface impurity groups (including F, OH, and SO_4) to relax surface energy, and they have a substantial influence on LA strength of Ti_{5C} sites on TiO_2 surfaces, which is closely related to photocatalytic activity.

It has been shown that the surface features play a crucial role in photocatalytic H_2 evolution[160]. According to the TMP-assisted solid-state NMR spectroscopy, it was found that the electron density of surface Ti_{5C} sites strongly decreased near the F ions, forming a dipole electric field ($F^{\delta-} \leftarrow Ti^{\delta+}$). The photogenerated holes and electrons can be efficiently separated under the action of the F-induced surface dipole electric field, which greatly prolongs the lifetime of the photogenerated carriers and, consequently, enhances photocatalytic activities. This point was further validated using a series of surface functional groups (–O–, F,

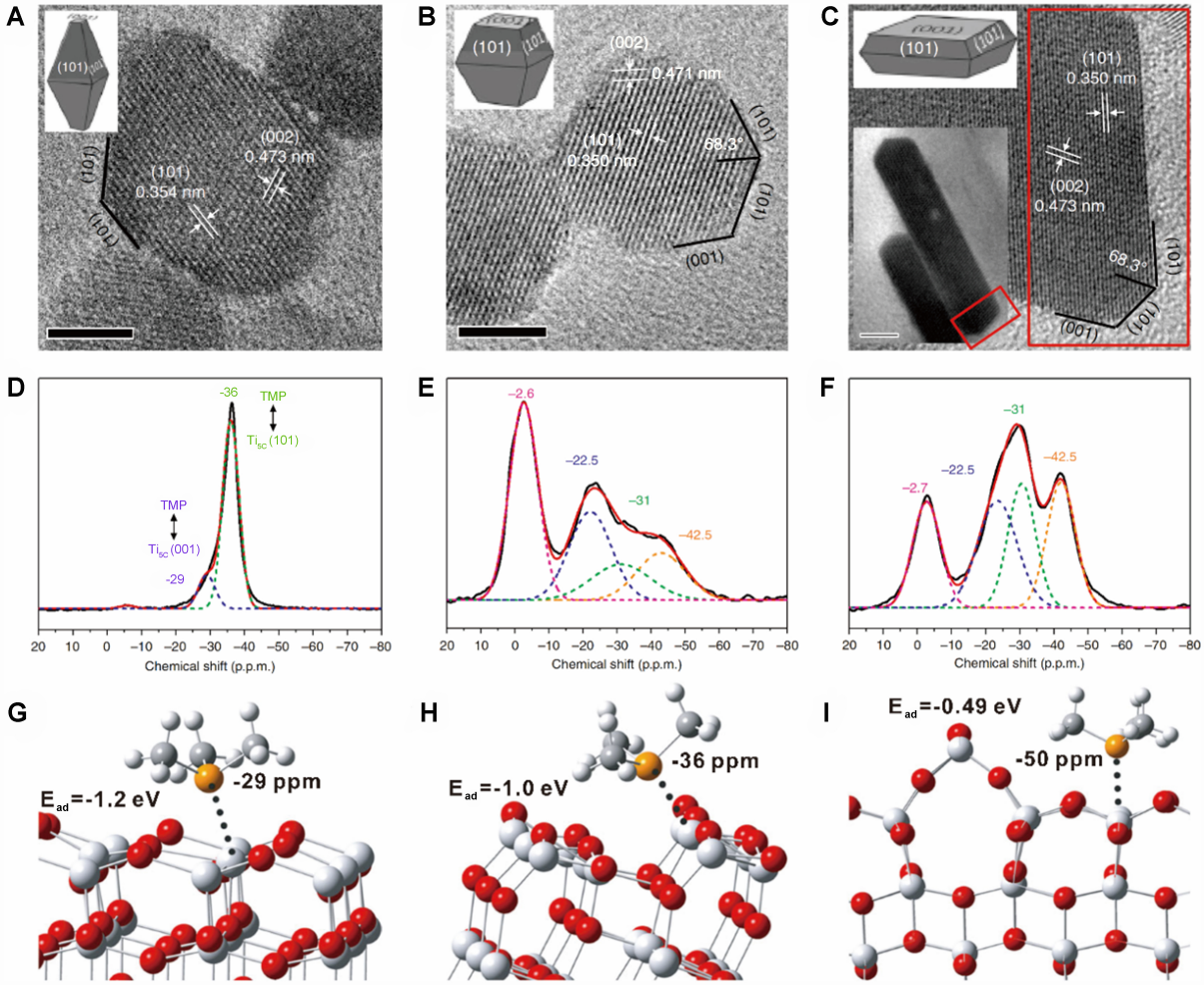

Figure 11. HRTEM images of as-prepared TiO_2 with (A) 90% and (B) 80% (101) facet, and (C) 75% (001) facet, and (D-F) their corresponding ^{31}P MAS NMR spectra of TMP-adsorbed TiO_2. Theoretical models and calculated adsorption energy (E_{ad}) between TMP and Ti_{5C} sites on various TiO_2 facets, including (G) (001) facet, (H) (101) facet, and (I) the reconstructed (1 × 4) (001) facet (Ti: light grey; O: red; P: orange; C: grey; H: white). Reproduced with permission from[164]. Copyright 2017, Springer Nature. HRTEM: High-resolution transmission electron microscopy; MAS: magic angle spinning; NMR: nuclear magnetic resonance; TMP: trimethylphosphine.

OH, and SO_4), which were systematically investigated by TMP-assisted ^{31}P NMR spectroscopy and DFT calculations[162,164]. The NMR spectra are sensitive to variations in the surface electronic properties for the series of TiO_2 samples [Figure 12A-C], and accordingly, a rational theoretical model is proposed. The highly sensitive ^{31}P chemical shift values correlate linearly and positively with the electron-withdrawing capacity of the surface functional groups to the Ti_{5C} sites (OH < –O– < SO_4 < F), indicating that these functional groups can provide fine-tuning of LA and BA sites on TiO_2 surface [Figure 12D and E]. Furthermore, the adsorption energies on surfaces modified by these functional groups (OH < –O– < SO_4 < F) show a linear relationship with ^{31}P chemical shift in the solid-state NMR spectra and the activity of photocatalytic H_2 evolution[162]. Moreover, the transfer process of photogenerated electrons is more efficient if the reactants are pre-adsorbed on the TiO_2 surface. Thus, the TMP-assisted ^{31}P NMR spectroscopy can sensitively probe surface electronic structure and properties, thus facilitating the design and development of efficient photocatalysts.

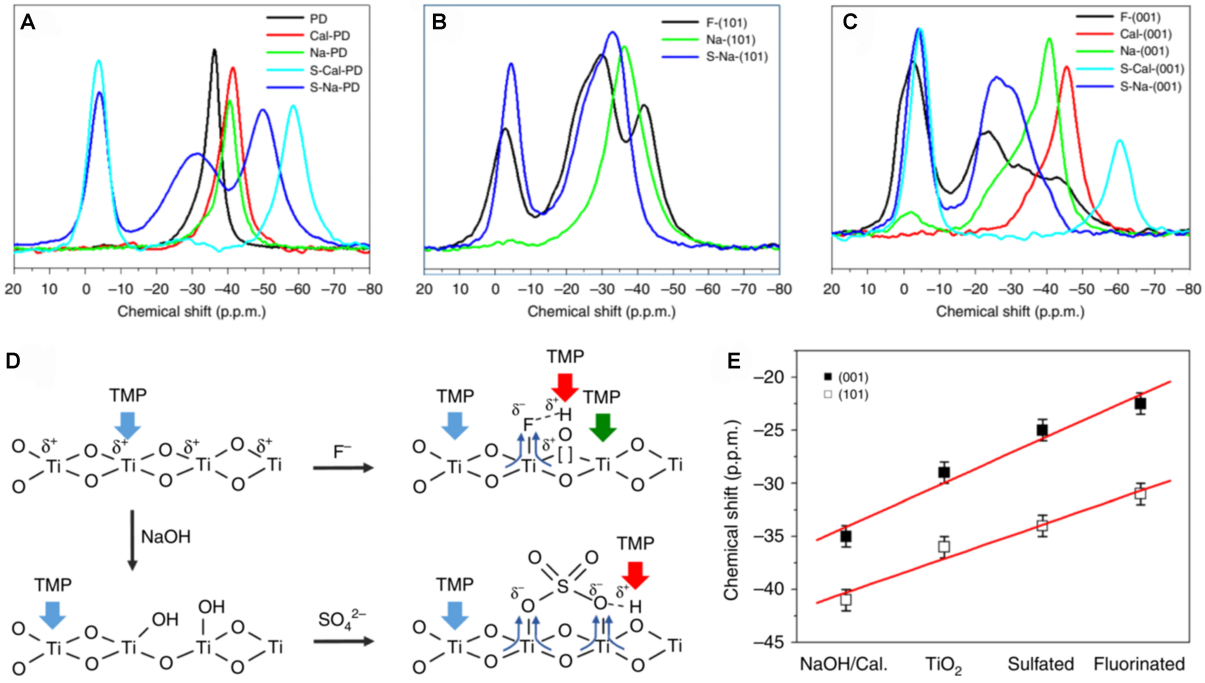

Figure 12. Summary of the electronic effect (chemical shift) imposed by different adsorbates during sequential treatments/modifications on (A) TiO_2 PD, (B) F-capped (101) facet [F-(101)], and (C) F-capped (001) facet [F-(001)]; (D) Illustration of interaction between TMP and surface features on TiO_2 facet with various treatments/modifications; (E) The summary of ^{31}P chemical shift of TMP-adsorbed Ti_{5C} on (001)/(101) facets with different treatments and modification. Reproduced with permission from[164]. Copyright 2017, Springer Nature. PD: powder; TMP: trimethylphosphine.

HETEROATOM ACTIVE SITES AND THEIR FUNCTION IN PHOTOCATALYSTS

The heteroatom (ions) doping should be one of the most promising methods to narrow the band gap and extend UV-light adsorption to the vis-light region. However, metallic doping (such as Al, V, and Ag) tends to be thermally unstable and inevitably introduces the recombination centers of photogenerated carriers[172-177]. On the other hand, the non-metallic doping (such as C, B, N, *etc.*) can introduce impurity bands located at 0.8-0.9 eV (i.e., below the conduction band bottom) due to the formation of localized oxygen vacancies[24,177-179], which results in a low electron mobility in anatase TiO_2. As such, although both metallic and non-metallic implantations can achieve vis-light absorption, they do not warrant enhanced photocatalytic activity of the doped TiO_2 photocatalysts. An in-depth understanding of heteroatoms (ions) sites and their mechanism is the prerequisite to establishing structure-activity relationship, which can promote the rational design of more efficient TiO_2 photocatalysts.

^{13}C-carbon

Carbon-doping of TiO_2 can efficiently enhance photocatalytic H_2 production, CO_2 reduction, and degradation of dyes and some small organic molecules under visible irradiation[180-185]. C-doped TiO_2 can be prepared by a simple sol-gel method using various carbon sources, including glucose, sucrose, and the titanium alkoxide precursor itself[186-191]. It has been confirmed that the structure and distribution of carbon species are closely correlated with the photocatalytic activity of C-doped TiO_2.

Rockafellow *et al.* achieved ^{13}C enrichment of carbon species in C-doped TiO_2 with ^{13}C-labeled glucose[192]. According to the one-dimensional (1D) ^{13}C MAS NMR spectra with spectral editing and 2D ^{13}C–^{13}C correlation NMR spectrum, the detailed six-carbon fragments were present in C-doped TiO_2 before annealing ($^{13}C_6$-TiO_2-0, Figure 13A and B). After annealing, the aromatic species were the main component

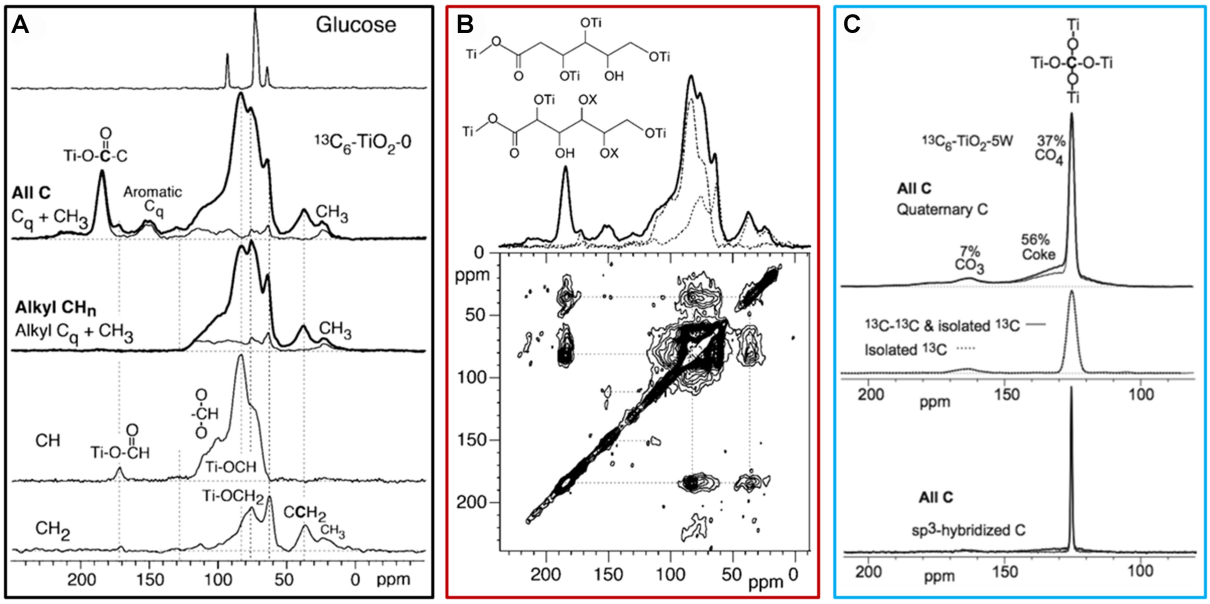

Figure 13. (A) ^{13}C NMR spectra of $^{13}C_6$-TiO_2-0. The spectrum of glucose for reference. Spectra of $^{13}C_6$-TiO_2-0 with spectral editing; (B) 2D ^{13}C–^{13}C correlation spectrum of $^{13}C_6$-TiO_2-0. Inserts: two structural fragments consistent with the observed cross peaks; (C) ^{13}C NMR spectra of $^{13}C_6$-TiO_2-5W: quantitative (DP) spectrum of all C and corresponding spectrum of nonprotonated C, J-modulated dephasing spectra, and selection of sp^3-hybridized C by a five-pulse CSA filter. Reproduced with permission from[192]. Copyright 2009, American Chemical Society. NMR: Nuclear magnetic resonance; 2D: two-dimensional; DP: direct polarization; CSA: chemical shift anisotropy.

of carbon species in the hybrid TiO_2 materials. Interestingly, when a washing step is added between the initial drying and annealing ($^{13}C_6$-TiO_2-5W), the major carbon species are transformed into an orthocarbonate structure, with C substituting Ti sites inside the TiO_2 [Figure 13C]. However, the reason for this change was still ambiguous. The authors found that the presence or absence of aromatic-carbon species on the TiO_2 surface was unrelated to the rate of photocatalytic degradation of quinoline, but had a significant effect on the product distribution. Instead, the reason for the high reactivity is presumed to be the formation of orthocarbonate centers.

We also reported a study of a minute quantity of carbon species doping on TiO_2 by using the titanium alkoxide precursor itself[190]. According to the ^{13}C MAS NMR experiments, the detailed structural changes of surface carbon species have been clarified [Figure 14]. After the C doping, four types of carbon species were observed, including carboxylate (182.9 ppm), graphite-like C (129 ppm), aromatics C (128.3 ppm), alkyl C (7.6-29.8 ppm). After washing the C-doped TiO_2 with HCl solution, the graphite-like C species should be the main carbon-containing component in the photocatalyst. It was found that graphite-like C species should be the active site to promote the separation of photogenerated carriers, resulting in high photocatalytic efficiency. In contrast, surface alkoxy and carboxylate C species would poison severely the C-doped TiO_2 surface and act as recombination centers of photogenerated carriers. The hole and electron transfer mechanism in the C-doped TiO_2 was proposed [Figure 14]. Most recently, we loaded graphene-like carbon nitride (g-C_3N_4) on TiO_2. According to solid-state NMR and XPS techniques, a strong coupling $(Ti)_2$–N–C bond is formed at the g-C_3N_4/TiO_2 interface, which efficiently facilitates the transfer of photogenerated carriers at the hybrid interface and efficient photocatalytic activity[193].

^{15}N-nitrogen

Nitrogen doping of TiO_2 can efficiently promote vis-light adsorption[24,194-199]. Reyes-Garcia *et al.* reported the detailed structure of nitrogen species in the N-doped TiO_2 prepared from different dopant precursors and

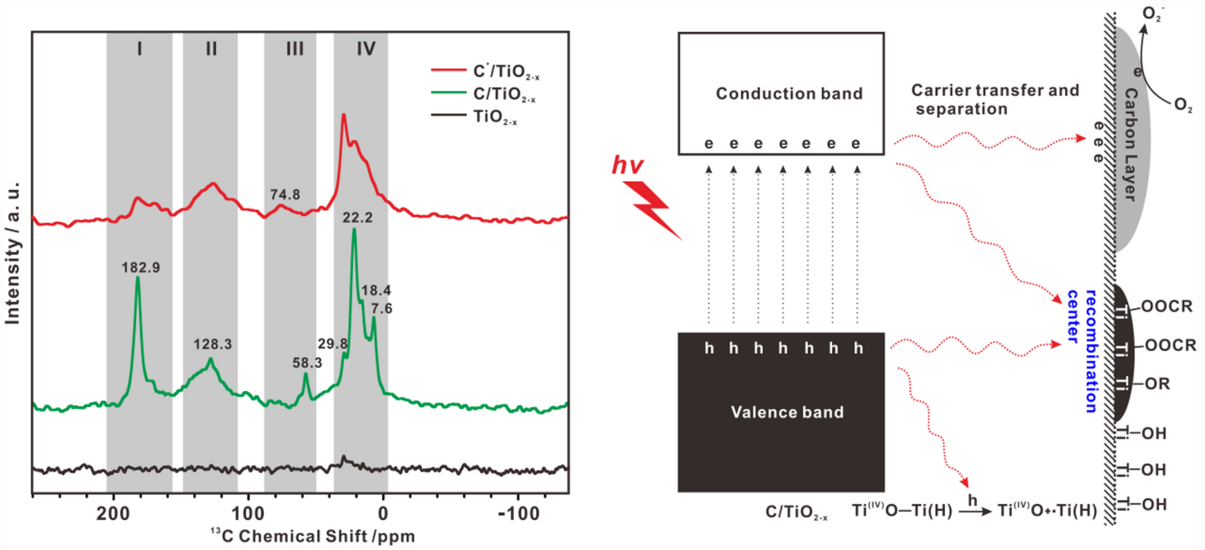

Figure 14. ^{13}C MAS NMR spectra of various C-doped TiO_2 samples (Right). Proposed hole and electron transfer mechanism in the C-doped TiO_2 photocatalyst (Left). Reproduced with permission from[190]. Copyright 2018, American Chemical Society. MAS: Magic angle spinning; NMR: nuclear magnetic resonance.

methods through ^{15}N solid-state NMR analysis[200]. As shown in Figure 15, three types of amino species (at -349.6, -355.1, and -369.5 ppm) were present in the ^{15}N-doped TiO_2 prepared by sol-gel methods and from $^{15}NH_4Cl$ as the dopant precursors. Two types of amino species (at -341.8 and -353 ppm) are also present in the ^{15}N-doped TiO_2 prepared by sol-gel methods and from ^{15}N-Urea as the dopant precursors. After calcination in air at 400, 500, or 550 °C, most of the amino-type N species were oxidized into nitrate species at ca. -6 ppm. The TiO_2 powders (P25) and monolayers were also nitrided and subjected to ^{15}N solid-state NMR analysis to determine the presence of nitridic bonds in these materials. However, besides the nitrate species, only the imido-type species (-150~-200 ppm) was present in the direct nitridation of TiO_2 [Figure 15B]. It was confirmed by the solid-state NMR results that the nitrogen atoms weave into the interstitial sites of N-doped TiO_2 in a highly oxidized state.

^{11}B-boron

The boron-doping can not only narrow the band gap of TiO_2 effectively to extend the absorption band to the vis-light region but also facilitate the separation of photogenerated carriers to promote photocatalytic activities[23,201-205]. Thus, the categories and structure of boron species have been extensively studied to gain their correlations with the photocatalytic properties. The conclusions of the aforementioned research were mostly obtained by XPS, which, however, remain controversial. For example, the XPS peaks at 190.5-191.8 eV were assigned to the B sites substituting the oxygen (O) sites of TiO_2[203,206-208], while the similar signals at 191.0-192.0 eV were ascribed to the B sites weaving into the interstitial sites of the TiO_2 lattice[201,202,209]. ^{11}B solid-state NMR spectroscopy is a powerful technique for providing detailed structural information on boron species in B-containing materials[23,201,202,210-213]. However, limited information was obtained in B-doped TiO_2 by using conventional ^{11}B Solid-State NMR techniques in the early days due to severe overlapping of the quadrupolar (I = 3/2) ^{11}B signals. The 2D multiple-quantum (MQ) MAS NMR has been used to remove the second-order quadrupolar interactions in the indirect dimension of solids containing quadrupolar nuclei[214-216]. However, for the tri-coordinated B species with large quadrupole coupling constants, the MQ technique was still unable to characterize the boron structure in B-doped TiO_2 photocatalysts with high resolution due to the low conversion efficiency from MQ to single-quantum coherences.

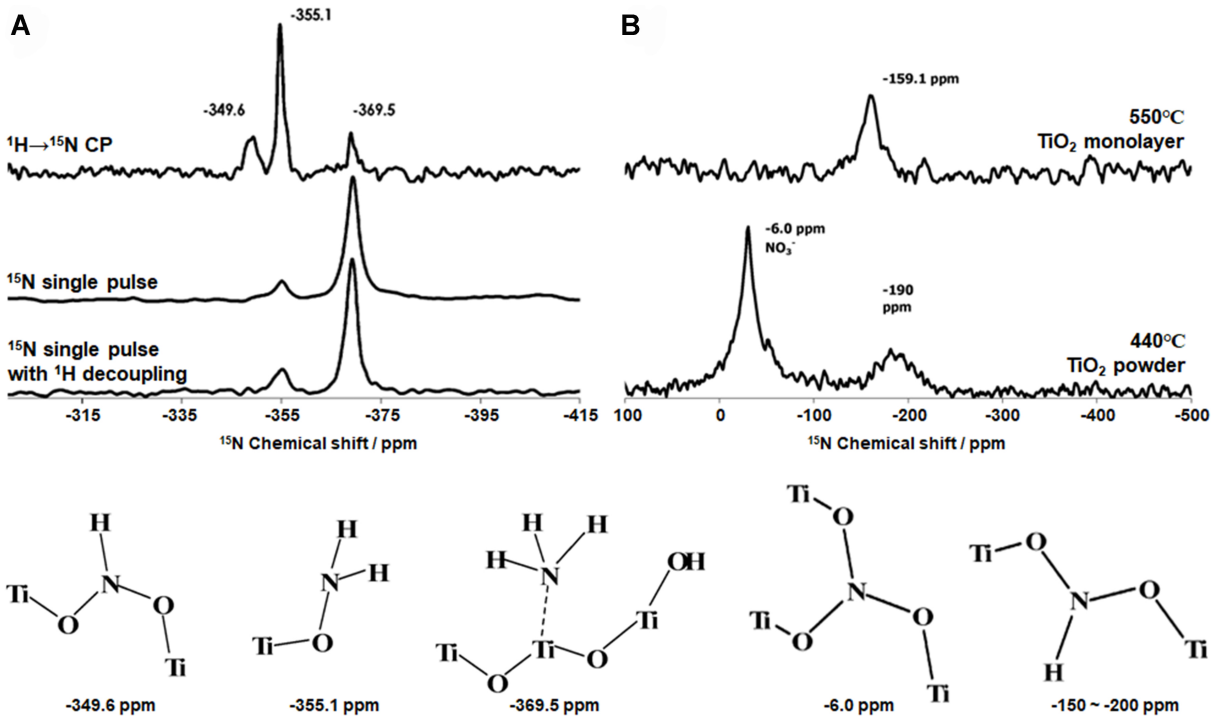

Figure 15. (A) ^{15}N MAS NMR spectra of ^{15}N-doped TiO_2 prepared by sol-gel methods; (B) ^{15}N MAS NMR spectra of ^{15}N-doped TiO_2 monolayer and powders by direct nitridation. Reproduced with permission from[200]. Copyright 2007, American Chemical Society. MAS: Magic angle spinning; NMR: nuclear magnetic resonance.

To gain more insights into the structure-activity relationship in photocatalytic reactions, we incorporated FAM RF pulse trains into the MQ MAS sequence, namely the so-called 3QZ-FAM MAS NMR technique, to improve the sensitivity of the ^{11}B NMR spectroscopy and investigate the detailed chemical environments of boron in B-doped and (B, Ag)-codoped TiO_2 photocatalysts [Figure 16A and B][202]. Up to five B sites were distinguished, corresponding to surface sites (B_5), small B polymer (B_2 and B_3), interstitial T^* (tri-coordinated, B_4), and Q^* (pseudo-tetrahedral coordinated, B_1) sites. Noteworthily, substituted B sites were absent in the materials. A 2D ^{11}B-^{11}B double-quantum (DQ) MAS NMR technique was first used to reveal the spatial distributions of the B sites in the B-doped and (B, Ag)-codoped TiO_2 photocatalysts [Figure 16C and D]. Accordingly, we found that only the tri-coordinated interstitial boron (T^*) species was near the substitutional Ag species to form [T^*–O–Ag] structural units. Combined with the evolution of the chemical states of the B and Ag dopants revealed by in-situ XPS experiments, a unique intermediate structure was formed by the [T^*–O–Ag] units trapping the photogenerated electron in the (B, Ag)-codoped TiO_2 during the irradiation as shown in Figure 17. To date, the developed 2D ^{11}B-^{11}B DQ Correlation NMR technique has been used to detect the spatial correlation of the B species in various B-containing materials, including boron nitride (BN), activated carbon impregnated with boric acid (B/OAC), boron-substituted MCM-22 zeolite (B-MWW) and silica-supported boron oxide (B/SiO_2)[39,212,213,217].

^{27}Al-aluminum

Although aluminum (Al)-doping cannot promote vis-light absorption, it would affect the crystal growth, cation diffusivity, and conductivity of TiO_2[176,218-220]. For photocatalysis, several contradictory results occurred due to the ambiguity of the structure-activity relationship of the Al sites in the Al-doped TiO_2 photocatalysts. Some reports found that Al doping could promote the separation of photogenerated carriers and thus improve photocatalytic activity[221-223]. On the other hand, others proposed that Al doping might

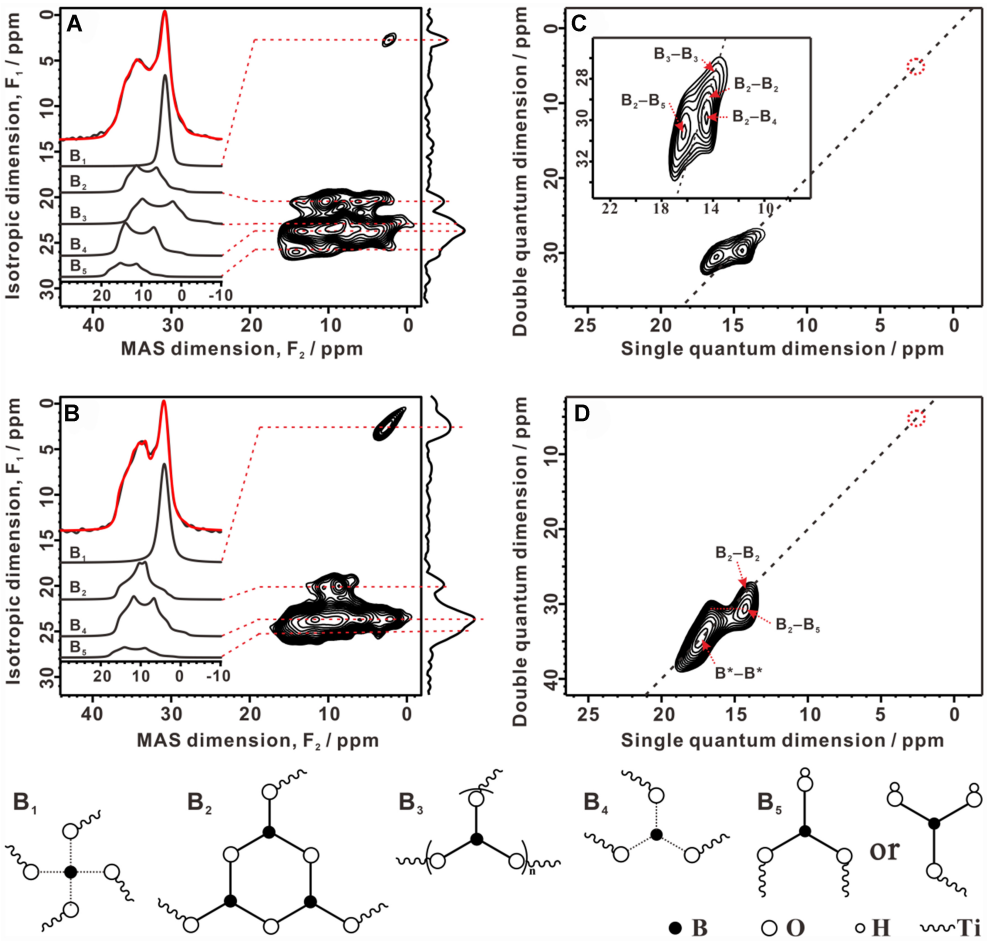

Figure 16. 2D ^{11}B 3QZ-FAM MAS NMR spectra (sheared) of (A) 10% B-doped and (B) (B, Ag)-codoped TiO_2 samples. 2D ^{11}B DQ MAS NMR spectra of (C) 10% B-doped and (D) (B, Ag)-codoped TiO_2 samples. Possible Boron Species in B-doped and (B, Ag)-codoped TiO_2 were shown at the bottom. Reproduced with permission from[202]. Copyright 2013, American Chemical Society. 2D: Two-dimensional; FAM: fast amplitude-modulated; MAS: magic angle spinning; NMR: nuclear magnetic resonance; DQ: double-quantum.

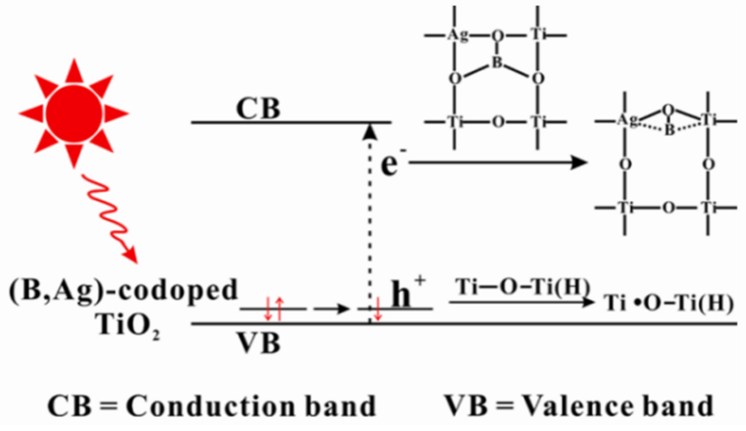

Figure 17. Electron/hole transfer mechanism for the (B, Ag)-codoped TiO_2 photocatalyst under irradiation from a solar-light source. Reproduced with permission from[202]. Copyright 2013, American Chemical Society.

introduce recombination centers of photogenerated carriers, which could have a negative impact on

photocatalytic activity[220,224]. Thus, it is essential to identify the active Al species in the Al-doped TiO_2.

To unravel the origins of the exceptional activity of Al-doped TiO_2 with dominant (001) facets [Al-$TiO_{2-x}F_x$ (001)], we employed advanced solid-state NMR methods to elucidate the fine structural details of the dopants, specifically F and Al species [Figure 18][225]. Notably, we first applied the 2D ^{19}F–^{27}Al dipolar heteronuclear multiple-quantum coherence (D-HMQC) NMR technique to probe F–Al proximity, enabling definitive confirmation of the F–Ti_2Al structural motif within the Al-$TiO_{2-x}F_x$(001) samples. According to the quantitative ^{19}F NMR measurements, the content of the F–Ti_2Al structure rises with greater Al doping, while that of other structures (including Ti–F–Ti, F–Ti_3, and Ti–F–Al) hardly increases. Combined with the spin-trapping electron spin resonance (ESR) results, it was found that the formation of the F–Ti_2Al structure promotes the separation and transfer of photogenerated carriers in the Al-$TiO_{2-x}F_x$(001) photocatalyst and is, therefore, considered to be the active site for photocatalytic reactions. However, with the further increase of Al doping, the oxygen vacancies occur, which should be the recombination centers of photogenerated carriers as reported in the previous work[176,220].

CONCLUSION AND OUTLOOK

Solid-state NMR spectroscopy can provide detailed information about the nature of the active centers and their structure-activity relationships in the TiO_2 photocatalysts. The local structure and coordination of different sites or species in the TiO_2 framework or on the TiO_2 surface can be identified by NMR chemical shift, owing to the high sensitivity of the NMR technique to the surrounding electronic environment. For example, bulk titanium and surface titanium can be distinguished by $^{47/49}Ti$ chemical shifts, and bulk oxygen, surface oxygen sites, hydroxyl groups, and adsorbed H_2O with different coordination states can be identified by ^{17}O chemical shifts. Surface electronic structure and properties, including the type, strength, and concentration of diverse adsorption sites, can be detected by probe-assisted NMR techniques. The correlation and connectivity of different sites or species in TiO_2 can be extracted from the specific internuclear interactions, including dipolar-dipolar and J-coupling interactions. Various advanced homonuclear/heteronuclear correlation NMR techniques based on dipole–dipole interaction or J-coupling have been developed to detect the dipolar-dipolar interactions for identifying internuclear proximities or chemical bonding, respectively[226,227]. For example, the spatial proximity between different active sites on hetero-atom (such as C, B, Al, *etc.*)-modified TiO_2 can be probed by 2D homonuclear (^{13}C–^{13}C/^{11}B–^{11}B) and heteronuclear (^{19}F–^{27}Al) correlation NMR spectra, while the 2D ^{1}H–^{11}B/^{17}O/$^{47/49}Ti$/^{95}Mo correlation NMR can identify the surface B/O/Ti/Mo site in the TiO_2 photocatalysts, which facilitate the solution of the complex surface structure.

Although remarkable progress has been achieved on the application and development of solid-state NMR methods, considerable challenges remain in TiO_2 photocatalysis for solid-state NMR characterization. It is difficult to detect dilute heteroatom sites and low-content surface/interface species (such as surface O and Ti sites) at high resolution. The intrinsic low sensitivity of solid-state NMR limits its application for this aspect, especially for some infamous nuclei with low natural abundances and low-γ features. All these active centers (including surface active sites and heteroatom sites) are fundamentally important in TiO_2 photocatalysis. Moreover, the complexity of complex surface structures, heteroatom distributions, and various covalent and non-covalent interactions in the TiO_2 photocatalysts leaves a huge space for advanced solid-state NMR techniques.

Our understanding of the complex structure of TiO_2 photocatalysts remains limited by the capabilities of existing solid-state NMR hardware and methodologies. An in-depth understanding of their structure-function relationships is essential for the further development of these fields. The increasing availability of

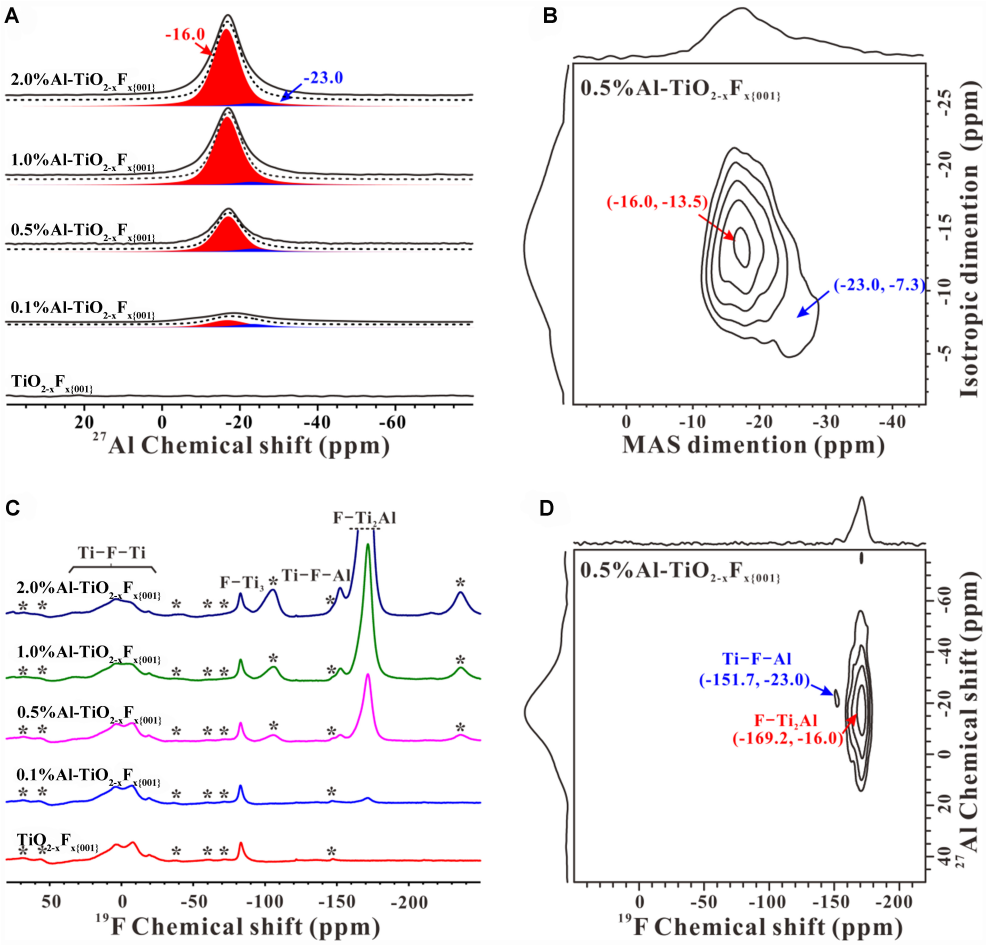

Figure 18. (A) 1D ^{27}Al MAS NMR spectra of $TiO_{2-x}F_x$(001) and Al–$TiO_{2-x}F_x$(001) catalysts; (B) 2D ^{27}Al 3Q MAS NMR spectrum of the Al–$TiO_{2-x}F_x$(001) sample; (C) 1D ^{19}F MAS NMR spectra of various of $TiO_{2-x}F_x$(001) and Al–$TiO_{2-x}F_x$(001) catalysts; (D) 2D ^{19}F–^{27}Al D-HMQC spectrum of the Al–$TiO_{2-x}F_x$(001) catalyst. Reproduced with permission from[225]. Copyright 2022, American Chemical Society. 1D: One-dimensional; MAS: magic angle spinning; NMR: nuclear magnetic resonance; 2D: two-dimensional; D-HMQC: dipolar heteronuclear multiple-quantum coherence.

ultra-high-field magnets and cryoprobes is improving solid-state NMR techniques to a higher level of detection sensitivity and resolution. Further development of sensitivity-enhanced 2D NMR techniques would enable the identification of the microstructure, distribution, and interaction of different active sites. Notably, the typical dopant elements used to modify TiO_2 photocatalysts, such as ^{51}V, ^{67}Zn, ^{71}Ga, ^{93}Nb, and ^{139}La, are characterized by low concentrations and substantial quadrupolar broadening of NMR spectral peaks. This significant line broadening results in an extremely low sensitivity of detection for these elements when using NMR as an analytical technique for studying doped TiO_2 photocatalysts. The utilization of hyperpolarization techniques such as DNP-NMR should be one of the most promising approaches to address such problems. The host-guest interactions typically occur in many important processes on TiO_2, such as the adsorption of H_2O/reactants and photocatalysis. The interaction between the framework nuclei (host) and the confined species (guest) can be probed by using double-resonance or 2D correlation NMR techniques. For example, 2D ^{1}H–^{1}H, ^{1}H–^{13}C, and ^{1}H–^{17}O correlation experiments can be used to characterize the interactions between surface hydroxyl/oxygen and adsorbed H_2O/organic compounds, which offer molecular-level insights into the photocatalytic mechanism (such as photocatalytic H_2O splitting) on TiO_2. Furthermore, in-situ solid-state NMR techniques can be developed to track the time evolution of reaction

intermediates. Therefore, the rapid progress of the solid-state NMR techniques would gain insight into the structure-property relationships in TiO_2 photocatalysts.

DECLARATIONS

Authors' contributions

Prepared and revised the manuscript: Feng N
Revised the manuscript: Feng N, Xu J, Deng F

Availability of data and materials

Not applicable.

Financial support and sponsorship

This work was supported by the National Natural Science Foundation of China (22372177, 22127801, 22225205, 22320102002, 22161132028), the Strategic Priority Research Program of the Chinese Academy of Sciences (XDB0540000), Natural Science Foundation of Hubei Province (S22H120101), Hubei International Scientific and Technological Cooperation Program (2022EHB021), and International Collaborative Center for Sustainable Catalysis and Magnetic Resonance (SH2303).

Conflicts of interest

Xu J served as editorial member of *Chemical Synthesis*, and he is Guest Editor of the Special Issue: "Advanced Characterization Techniques and Applications for Catalytic Materials", while the other authors have declared that they have no conflicts of interest.

Ethical approval and consent to participate

Not applicable.

Consent for publication

Not applicable.

REFERENCES

1. Ruan X, Li S, Huang C, Zheng W, Cui X, Ravi SK. Catalyzing artificial photosynthesis with TiO_2 heterostructures and hybrids: emerging trends in a classical yet contemporary photocatalyst. *Adv Mater* 2024;36:e2305285. DOI PubMed
2. Fujishima A, Honda K. Electrochemical photolysis of water at a semiconductor electrode. *Nature* 1972;238:37-8. DOI PubMed
3. Tang R, Zhou S, Zhang Z, Zheng R, Huang J. Engineering nanostructure-interface of photoanode materials toward photoelectrochemical water oxidation. *Adv Mater* 2021;33:e2005389. DOI PubMed
4. Warnan J, Reisner E. Synthetic organic design for solar fuel systems. *Angew Chem Int Ed Engl* 2020;59:17344-54. DOI PubMed PMC
5. Wang Z, Hisatomi T, Li R, et al. Efficiency accreditation and testing protocols for particulate photocatalysts toward solar fuel production. *Joule* 2021;5:344-59. DOI
6. Ismail AA, Bahnemann DW. Photochemical splitting of water for hydrogen production by photocatalysis: a review. *Sol Energy Mater Sol Cells* 2014;128:85-101. DOI
7. Rawool SA, Yadav KK, Polshettiwar V. Defective TiO_2 for photocatalytic CO_2 conversion to fuels and chemicals. *Chem Sci* 2021;12:4267-99. DOI PubMed PMC
8. Morikawa T, Sato S, Sekizawa K, Suzuki TM, Arai T. Solar-driven CO_2 reduction using a semiconductor/molecule hybrid photosystem: from photocatalysts to a monolithic artificial leaf. *Acc Chem Res* 2022;55:933-43. DOI PubMed
9. Li Y, Lei Y, Li D, et al. Recent progress on photocatalytic CO_2 conversion reactions over plasmonic metal-based catalysts. *ACS Catal* 2023;13:10177-204. DOI
10. Lin Z, Jiang X, Xu W, et al. The effects of water, substrate, and intermediate adsorption on the photocatalytic decomposition of air

pollutants over nano-TiO_2 photocatalysts. *Phys Chem Chem Phys* 2024;26:662-78. DOI PubMed

11. Wu H, Li L, Wang S, et al. Recent advances of semiconductor photocatalysis for water pollutant treatment: mechanisms, materials and applications. *Phys Chem Chem Phys* 2023;25:25899-924. DOI PubMed
12. Linsebigler AL, Lu G, Yates JT. Photocatalysis on TiO_2 surfaces: principles, mechanisms, and selected results. *Chem Rev* 1995;95:735-58. DOI
13. Chen LX, Rajh T, Jäger W, Nedeljkovic J, Thurnauer MC. X-ray absorption reveals surface structure of titanium dioxide nanoparticles. *J Synchrotron Radiat* 1999;6:445-7. DOI PubMed
14. Selloni A. Crystal growth: anatase shows its reactive side. *Nat Mater* 2008;7:613-5. DOI PubMed
15. Pan J, Liu G, Lu GQ, Cheng HM. On the true photoreactivity order of {001}, {010}, and {101} facets of anatase TiO_2 crystals. *Angew Chem Int Ed Engl* 2011;50:2133-7. DOI PubMed
16. Yang HG, Sun CH, Qiao SZ, et al. Anatase TiO_2 single crystals with a large percentage of reactive facets. *Nature* 2008;453:638-41. DOI PubMed
17. Feng N, Lin H, Song H, et al. Efficient and selective photocatalytic CH_4 conversion to CH_3OH with O_2 by controlling overoxidation on TiO_2. *Nat Commun* 2021;12:4652. DOI PubMed PMC
18. Yu J, Zhao X, Zhao Q. Effect of film thickness on the grain size and photocatalytic activity of the sol-gel derived nanometer TiO_2 thin films. *J Mater Sci Lett* 2000;19:1015-7. DOI
19. Zhu J, Liao M, Zhao C, et al. A comprehensive review on semiconductor-based photocatalysts toward the degradation of persistent pesticides. *Nano Res* 2023;16:6402-43. DOI
20. Chen F, Ma T, Zhang T, Zhang Y, Huang H. Atomic-level charge separation strategies in semiconductor-based photocatalysts. *Adv Mater* 2021;33:e2005256. DOI PubMed
21. Wang H, Liu W, He X, Zhang P, Zhang X, Xie Y. An excitonic perspective on low-dimensional semiconductors for photocatalysis. *J Am Chem Soc* 2020;142:14007-22. DOI PubMed
22. Liu N, Schneider C, Freitag D, et al. Black TiO_2 nanotubes: cocatalyst-free open-circuit hydrogen generation. *Nano Lett* 2014;14:3309-13. DOI PubMed
23. Wang F, Jiang Y, Gautam A, Li Y, Amal R. Exploring the origin of enhanced activity and reaction pathway for photocatalytic H_2 production on Au/B-TiO_2 catalysts. *ACS Catal* 2014;4:1451-7. DOI
24. Asahi R, Morikawa T, Ohwaki T, Aoki K, Taga Y. Visible-light photocatalysis in nitrogen-doped titanium oxides. *Science* 2001;293:269-71. DOI PubMed
25. Chen S, Hu YH. Color TiO_2 materials as emerging catalysts for visible-NIR light photocatalysis, a review. *Catal Rev* 2023. DOI
26. Li X, Wu X, Liu S, Li Y, Fan J, Lv K. Effects of fluorine on photocatalysis. *Chin J Catal* 2020;41:1451-67. DOI
27. Peiris S, de Silva HB, Ranasinghe KN, Bandara SV, Perera IR. Recent development and future prospects of TiO_2 photocatalysis. *J Chin Chem Soc* 2021;68:738-69. DOI
28. Xiu Z, Guo M, Zhao T, et al. Recent advances in Ti^{3+} self-doped nanostructured TiO_2 visible light photocatalysts for environmental and energy applications. *Chem Eng J* 2020;382:123011. DOI
29. Medhi R, Marquez MD, Lee TR. Visible-light-active doped metal oxide nanoparticles: review of their synthesis, properties, and applications. *ACS Appl Nano Mater* 2020;3:6156-85. DOI
30. Kovačič Ž, Likozar B, Huš M. Photocatalytic CO_2 reduction: a review of ab initio mechanism, kinetics, and multiscale modeling simulations. *ACS Catal* 2020;10:14984-5007. DOI
31. Wu S, Lin Y, Hu YH. Strategies of tuning catalysts for efficient photodegradation of antibiotics in water environments: a review. *J Mater Chem A* 2021;9:2592-611. DOI
32. Rahman MZ, Raziq F, Zhang H, Gascon J. Key strategies for enhancing H_2 production in transition metal oxide based photocatalysts. *Angew Chem Int Ed Engl* 2023;62:e202305385. DOI PubMed
33. Chakhtouna H, Benzeid H, Zari N, Qaiss AEK, Bouhfid R. Recent progress on Ag/TiO_2 photocatalysts: photocatalytic and bactericidal behaviors. *Environ Sci Pollut Res Int* 2021;28:44638-66. DOI PubMed PMC
34. Li X, Wei H, Song T, Lu H, Wang X. A review of the photocatalytic degradation of organic pollutants in water by modified TiO_2. *Water Sci Technol* 2023;88:1495-507. DOI PubMed
35. Yao S, He J, Gao F, et al. Highly selective semiconductor photocatalysis for CO_2 reduction. *J Mater Chem A* 2023;11:12539-58. DOI
36. Lee D, Kim M, Danish M, Jo W. State-of-the-art review on photocatalysis for efficient wastewater treatment: attractive approach in photocatalyst design and parameters affecting the photocatalytic degradation. *Catal Commun* 2023;183:106764. DOI
37. Lin S, Huang H, Ma T, Zhang Y. Photocatalytic oxygen evolution from water splitting. *Adv Sci* 2020;8:2002458. DOI PubMed PMC
38. Cao Y, Zhou P, Tu Y, et al. Modification of TiO_2 nanoparticles with organodiboron molecules inducing stable surface Ti^{3+} complex. *iScience* 2019;20:195-204. DOI PubMed PMC
39. Jung D, Saleh LMA, Berkson ZJ, et al. A molecular cross-linking approach for hybrid metal oxides. *Nat Mater* 2018;17:341-8. DOI PubMed
40. Kowalska E, Yoshiiri K, Wei Z, et al. Hybrid photocatalysts composed of titania modified with plasmonic nanoparticles and ruthenium complexes for decomposition of organic compounds. *Appl Catal B Environ* 2015;178:133-43. DOI
41. Rengifo-herrera JA, Blanco M, Wist J, Florian P, Pizzio LR. TiO_2 modified with polyoxotungstates should induce visible-light

absorption and high photocatalytic activity through the formation of surface complexes. *Appl Catal B Environ* 2016;189:99-109. DOI

42. Liu F, Feng N, Wang Q, et al. Transfer channel of photoinduced holes on a TiO_2 surface as revealed by solid-state nuclear magnetic resonance and electron spin resonance spectroscopy. *J Am Chem Soc* 2017;139:10020-8. DOI PubMed
43. Jaeger CD, Bard AJ. Spin trapping and electron spin resonance detection of radical intermediates in the photodecomposition of water at titanium dioxide particulate systems. *J Phys Chem* 1979;83:3146-52. DOI
44. Nosaka Y, Komori S, Yawata K, Hirakawa T, Nosaka AY. Photocatalytic ˙OH radical formation in TiO_2 aqueous suspension studied by several detection methods. *Phys Chem Chem Phys* 2003;5:4731-5. DOI
45. Liu G, Yang HG, Wang X, et al. Visible light responsive nitrogen doped anatase TiO_2 sheets with dominant {001} facets derived from TiN. *J Am Chem Soc* 2009;131:12868-9. DOI PubMed
46. Ishibashi K, Fujishima A, Watanabe T, Hashimoto K. Quantum yields of active oxidative species formed on TiO_2 photocatalyst. *J Photoch Photobio A* 2000;134:139-42. DOI
47. Guan H, Lin J, Qiao B, et al. Catalytically active Rh sub-nanoclusters on TiO_2 for CO oxidation at cryogenic temperatures. *Angew Chem Int Ed Engl* 2016;55:2820-4. DOI PubMed
48. Wu N, Wang J, Tafen de N, et al. Shape-enhanced photocatalytic activity of single-crystalline anatase TiO_2 (101) nanobelts. *J Am Chem Soc* 2010;132:6679-85. DOI PubMed PMC
49. Micic OI, Zhang Y, Cromack KR, Trifunac AD, Thurnauer MC. Trapped holes on titania colloids studied by electron paramagnetic resonance. *J Phys Chem* 1993;97:7277-83. DOI
50. Yang L, Feng N, Wang Q, Chu Y, Xu J, Deng F. Surface water loading on titanium dioxide modulates photocatalytic water splitting. *Cell Rep Phys Sci* 2020;1:100013. DOI
51. Yuan W, Zhu B, Fang K, et al. In situ manipulation of the active Au-TiO_2 interface with atomic precision during CO oxidation. *Science* 2021;371:517-21. DOI PubMed
52. Song S, Song H, Li L, et al. A selective Au-ZnO/TiO_2 hybrid photocatalyst for oxidative coupling of methane to ethane with dioxygen. *Nat Catal* 2021;4:1032-42. DOI
53. Monai M, Jenkinson K, Melcherts AEM, et al. Restructuring of titanium oxide overlayers over nickel nanoparticles during catalysis. *Science* 2023;380:644-51. DOI PubMed
54. Xu M, Qin X, Xu Y, et al. Boosting CO hydrogenation towards C_{2+} hydrocarbons over interfacial TiO_{2-x}/Ni catalysts. *Nat Commun* 2022;13:6720. DOI PubMed PMC
55. Wei J, Qin SN, Liu JL, et al. In situ raman monitoring and manipulating of interfacial hydrogen spillover by precise fabrication of Au/TiO_2/Pt sandwich structures. *Angew Chem Int Ed Engl* 2020;59:10343-7. DOI PubMed
56. Zhu K, Zhu Q, Jiang M, et al. Modulating Ti t_{2g} orbital occupancy in a Cu/TiO_2 composite for selective photocatalytic CO_2 reduction to CO. *Angew Chem Int Ed Engl* 2022;61:e202207600. DOI PubMed
57. Balajka J, Hines MA, DeBenedetti WJI, et al. High-affinity adsorption leads to molecularly ordered interfaces on TiO_2 in air and solution. *Science* 2018;361:786-9. DOI PubMed
58. Guo Y, Huang Y, Zeng B, et al. Photo-thermo semi-hydrogenation of acetylene on Pd_1/TiO_2 single-atom catalyst. *Nat Commun* 2022;13:2648. DOI PubMed PMC
59. Chen Y, Soler L, Cazorla C, et al. Facet-engineered TiO_2 drives photocatalytic activity and stability of supported noble metal clusters during H_2 evolution. *Nat Commun* 2023;14:6165. DOI PubMed PMC
60. Len T, Afanasiev P, Yan Y, Aouine M, Morfin F, Piccolo L. Operando X-ray absorption spectroscopic study of ultradispersed Mo/TiO_2 CO_2-hydrogenation catalysts: why does rutile promote methanol synthesis? *ACS Catal* 2023;13:13982-93. DOI
61. Berger T, Sterrer M, Diwald O, et al. Light-induced charge separation in anatase TiO_2 particles. *J Phys Chem B* 2005;109:6061-8. DOI PubMed
62. Nakamura R, Imanishi A, Murakoshi K, Nakato Y. In situ FTIR studies of primary intermediates of photocatalytic reactions on nanocrystalline TiO_2 films in contact with aqueous solutions. *J Am Chem Soc* 2003;125:7443-50. DOI PubMed
63. Copéret C, Liao WC, Gordon CP, Ong TC. Active sites in supported single-site catalysts: an NMR perspective. *J Am Chem Soc* 2017;139:10588-96. DOI PubMed
64. Xu J, Wang Q, Deng F. Metal active sites and their catalytic functions in zeolites: insights from solid-state NMR spectroscopy. *Acc Chem Res* 2019;52:2179-89. DOI PubMed
65. Ashbrook SE, Sneddon S. New methods and applications in solid-state NMR spectroscopy of quadrupolar nuclei. *J Am Chem Soc* 2014;136:15440-56. DOI PubMed
66. Kwak JH, Hu J, Mei D, et al. Coordinatively unsaturated Al^{3+} centers as binding sites for active catalyst phases of platinum on γ-Al_2O_3. *Science* 2009;325:1670-3. DOI PubMed
67. Wang Q, Li W, Hung I, et al. Mapping the oxygen structure of γ-Al_2O_3 by high-field solid-state NMR spectroscopy. *Nat Commun* 2020;11:3620. DOI PubMed PMC
68. Peng L, Liu Y, Kim N, Readman JE, Grey CP. Detection of Brønsted acid sites in zeolite HY with high-field ^{17}O-MAS-NMR techniques. *Nat Mater* 2005;4:216-9. DOI PubMed
69. Ashbrook SE, Smith ME. Solid state ^{17}O NMR-an introduction to the background principles and applications to inorganic materials. *Chem Soc Rev* 2006;35:718-35. DOI PubMed
70. Wang M, Wu XP, Zheng S, et al. Identification of different oxygen species in oxide nanostructures with ^{17}O solid-state NMR

spectroscopy. *Sci Adv* 2015;1:e1400133. DOI PubMed PMC
71. Beck TJ, Klust A, Batzill M, Diebold U, Di Valentin C, Selloni A. Surface structure of TiO_2(011)-(2×1). *Phys Rev Lett* 2004;93:036104. DOI PubMed
72. Di Valentin C, Tilocca A, Selloni A, et al. Adsorption of water on reconstructed rutile TiO_2(011)-(2 × 1): Ti=O double bonds and surface reactivity. *J Am Chem Soc* 2005;127:9895-903. DOI PubMed
73. He Y, Tilocca A, Dulub O, Selloni A, Diebold U. Local ordering and electronic signatures of submonolayer water on anatase TiO_2 (101). *Nat Mater* 2009;8:585-9. DOI PubMed
74. Yuan W, Zhu B, Li XY, et al. Visualizing H_2O molecules reacting at TiO_2 active sites with transmission electron microscopy. *Science* 2020;367:428-30. DOI PubMed
75. Aronson BJ, Blanford CF, Stein A. Solution-phase grafting of titanium dioxide onto the pore surface of mesoporous silicates: synthesis and structural characterization. *Chem Mater* 1997;9:2842-51. DOI
76. Shukri G, Kasai H. Density functional theory study of ethylene adsorption on clean anatase TiO_2 (001) surface. *Surf Sci* 2014;619:59-66. DOI
77. Sanz JF, Hernández NC, Márquez A. A first principles study of Pd deposition on the TiO_2 (110) surface. *TheorChem Acc* 2000;104:317-22. DOI
78. Zhou G, Jiang L, Dong Y, Li R, He D. Engineering the exposed facets and open-coordinated sites of brookite TiO_2 to boost the loaded Ru nanoparticle efficiency in benzene selective hydrogenation. *Appl Surf Sci* 2019;486:187-97. DOI
79. Vijay A, Mills G, Metiu H. Adsorption of gold on stoichiometric and reduced rutile TiO_2(110) surfaces. *J Chem Phys* 2003;118:6536-51. DOI
80. Posternak M, Baldereschi A, Delley B. Dissociation of water on anatase TiO_2 nanoparticles: the role of undercoordinated Ti atoms at edges. *J Phys Chem C* 2009;113:15862-7. DOI
81. Dette C, Pérez-osorio MA, Mangel S, Giustino F, Jung SJ, Kern K. Atomic structure of water monolayer on anatase TiO_2 (101) surface. *J Phys Chem C* 2018;122:11954-60. DOI
82. Dette C, Pérez-osorio MA, Mangel S, Giustino F, Jung SJ, Kern K. Single-molecule vibrational spectroscopy of H_2O on anatase TiO_2 (101). *J Phys Chem C* 2017;121:1182-7. DOI
83. Gopal NO, Lo HH, Sheu SC, Ke SC. A potential site for trapping photogenerated holes on rutile TiO_2 surface as revealed by EPR spectroscopy: an avenue for enhancing photocatalytic activity. *J Am Chem Soc* 2010;132:10982-3. DOI PubMed
84. Nolan M, Iwaszuk A, Gray KA. Localization of photoexcited electrons and holes on low coordinated Ti and O sites in free and supported TiO_2 nanoclusters. *J Phys Chem C* 2014;118:27890-900. DOI
85. Xiong F, Yu YY, Wu Z, et al. Methanol conversion into dimethyl ether on the anatase TiO_2(001) surface. *Angew Chem Int Ed Engl* 2016;55:623-8. DOI PubMed
86. Dmitrieva LV, Vorotilova LS, Podkorytov IS, Shelyapina ME. A comparison of NMR spectral parameters of ^{47}Ti and ^{49}Ti nuclei in rutile and anatase. *Phys Solid State* 1999;41:1097-9. DOI
87. Ganapathy S, Gore KU, Kumar R, Amoureux JP. Multinuclear (^{27}Al, ^{29}Si, ^{47,49}Ti) solid-state NMR of titanium substituted zeolite USY. *Solid State Nucl Magn Reson* 2003;24:184-95. DOI PubMed
88. Yamada K, Saito M, Ohashi R, Nakai T, Deguchi K, Shimizu T. Solid-state $^{47/49}$Ti nuclear magnetic resonance of TiO_2. *Chem Lett* 2014;43:1520-1. DOI
89. Quantities, units and symbols in physical chemistry. 2nd editon. 1993. Available from: https://old.iupac.org/publications/books/gbook/green_book_2ed.pdf. [Last accessed on 5 Jul 2024].
90. Stone NJ. Table of nuclear electric quadrupole moments. *Atom Data Nucl Data* 2016;111-2:1-28. DOI
91. Pyykkö P. Year-2008 nuclear quadrupole moments. *Mol Phys* 2008;106:1965-74. DOI
92. Bastow TJ, Whitfield HJ. ^{47,49}Ti NMR: evolution of crystalline TiO_2 from the gel state. *Chem Mater* 1999;11:3518-20. DOI
93. Gervais C, Smith ME, Pottier A, Jolivet J, Babonneau F. Solid-State ^{47,49}Ti NMR determination of the phase distribution of titania nanoparticles. *Chem Mater* 2001;13:462-7. DOI
94. Bräuniger T, Madhu PK, Pampel A, Reichert D. Application of fast amplitude-modulated pulse trains for signal enhancement in static and magic-angle-spinning ^{47,49}Ti-NMR spectra. *Solid State Nucl Magn Reson* 2004;26:114-20. DOI PubMed
95. Larsen FH, Farnan I, Lipton AS. Separation of ^{47}Ti and ^{49}Ti solid-state NMR lineshapes by static QCPMG experiments at multiple fields. *J Magn Reson* 2006;178:228-36. DOI PubMed
96. Epifani M, Comini E, Díaz R, Force C, Siciliano P, Faglia G. TiO_2 colloidal nanocrystals surface modification by V_2O_5 species: Investigation by ^{47,49}Ti MAS-NMR and H_2, CO and NO_2 sensing properties. *Appl Surf Sci* 2015;351:1169-73. DOI
97. Gerothanassis IP. Oxygen-17 NMR spectroscopy: basic principles and applications (part I). *Prog Nucl Magn Reson Spectrosc* 2010;56:95-197. DOI PubMed
98. Gerothanassis IP. Oxygen-17 NMR spectroscopy: basic principles and applications. Part II. *Prog Nucl Magn Reson Spectrosc* 2010;57:1-110. DOI PubMed
99. Bastow TJ, Doran G, Whitfield HJ. Electron diffraction and ^{47,49}Ti and ^{17}O NMR studies of natural and synthetic brookite. *Chem Mater* 2000;12:436-9. DOI
100. Lafond V, Gervais C, Maquet J, Prochnow D, Babonneau F, Mutin PH. ^{17}O MAS NMR study of the bonding mode of phosphonate coupling molecules in a titanium oxo-alkoxo-phosphonate and in titania-based hybrid materials. *Chem Mater* 2003;15:4098-103. DOI

101. Bastow TJ, Moodie AF, Smith ME, Whitfield HJ. Characterisation of titania gels by ^{17}O nuclear magnetic resonance and electron diffraction. *J Mater Chem* 1993;3:697. DOI
102. Rao Y, Kemp TF, Trudeau M, Smith ME, Antonelli DM. ^{17}O and ^{15}N solid state NMR studies on ligand-assisted templating and oxygen coordination in the walls of mesoporous Nb, Ta and Ti oxides. *J Am Chem Soc* 2008;130:15726-31. DOI PubMed
103. Métro TX, Gervais C, Martinez A, Bonhomme C, Laurencin D. Unleashing the potential of ^{17}O NMR spectroscopy using mechanochemistry. *Angew Chem Int Ed Engl* 2017;56:6803-7. DOI PubMed
104. Sun X, Dyballa M, Yan J, Li L, Guan N, Hunger M. Solid-state NMR investigation of the $^{16/17}$O isotope exchange of oxygen species in pure-anatase and mixed-phase TiO_2. *Chem Phys Lett* 2014;594:34-40. DOI
105. Li Y, Wu XP, Jiang N, et al. Distinguishing faceted oxide nanocrystals with ^{17}O solid-state NMR spectroscopy. *Nat Commun* 2017;8:581. DOI PubMed PMC
106. Li Y, Wu XP, Liu C, et al. NMR and EPR studies of partially reduced TiO_2. *Acta Phys Chim Sin* 2020;36:1905021. DOI
107. Peng L, Huo H, Liu Y, Grey CP. ^{17}O magic angle spinning NMR studies of Brønsted acid sites in zeolites HY and HZSM-5. *J Am Chem Soc* 2007;129:335-46. DOI PubMed
108. Merle N, Trébosc J, Baudouin A, et al. ^{17}O NMR gives unprecedented insights into the structure of supported catalysts and their interaction with the silica carrier. *J Am Chem Soc* 2012;134:9263-75. DOI PubMed
109. Guo Q, Ma Z, Zhou C, Ren Z, Yang X. Single molecule photocatalysis on TiO_2 surfaces. *Chem Rev* 2019;119:11020-41. DOI PubMed
110. Chen J, Hope MA, Lin Z, et al. Interactions of oxide surfaces with water revealed with solid-state NMR spectroscopy. *J Am Chem Soc* 2020;142:11173-82. DOI PubMed
111. Ravera E, Luchinat C, Parigi G. Basic facts and perspectives of Overhauser DNP NMR. *J Magn Reson* 2016;264:78-87. DOI PubMed
112. Gurinov A, Sieland B, Kuzhelev A, et al. Mixed-valence compounds as polarizing agents for overhauser dynamic nuclear polarization in solids*. *Angew Chem Int Ed Engl* 2021;60:15371-5. DOI PubMed PMC
113. Küçük SE, Biktagirov T, Sezer D. Carbon and proton Overhauser DNP from MD simulations and ab initio calculations: TEMPOL in acetone. *Phys Chem Chem Phys* 2015;17:24874-84. DOI PubMed
114. Wiśniewski D, Karabanov A, Lesanovsky I, Köckenberger W. Solid effect DNP polarization dynamics in a system of many spins. *J Magn Reson* 2016;264:30-8. DOI PubMed
115. Banerjee D, Shimon D, Feintuch A, Vega S, Goldfarb D. The interplay between the solid effect and the cross effect mechanisms in solid state ^{13}C DNP at 95 GHz using trityl radicals. *J Magn Reson* 2013;230:212-9. DOI PubMed
116. Liao W, Ghaffari B, Gordon CP, Xu J, Copéret C. Dynamic nuclear polarization surface enhanced NMR spectroscopy (DNP SENS): principles, protocols, and practice. *Curr Opin Colloid In* 2018;33:63-71. DOI
117. Park H, Uluca-Yazgi B, Heumann S, et al. Heteronuclear cross-relaxation effect modulated by the dynamics of N-functional groups in the solid state under ^{15}N DP-MAS DNP. *J Magn Reson* 2020;312:106688. DOI PubMed
118. Hovav Y, Feintuch A, Vega S. Theoretical aspects of dynamic nuclear polarization in the solid state - the cross effect. *J Magn Reson* 2012;214:29-41. DOI PubMed
119. Rankin AGM, Trébosc J, Pourpoint F, Amoureux JP, Lafon O. Recent developments in MAS DNP-NMR of materials. *Solid State Nucl Magn Reson* 2019;101:116-43. DOI PubMed
120. Lesage A, Lelli M, Gajan D, et al. Surface enhanced NMR spectroscopy by dynamic nuclear polarization. *J Am Chem Soc* 2010;132:15459-61. DOI PubMed
121. Rossini AJ, Zagdoun A, Lelli M, Lesage A, Copéret C, Emsley L. Dynamic nuclear polarization surface enhanced NMR spectroscopy. *Acc Chem Res* 2013;46:1942-51. DOI PubMed
122. Kobayashi T, Perras FA, Slowing II, Sadow AD, Pruski M. Dynamic nuclear polarization solid-state NMR in heterogeneous catalysis research. *ACS Catal* 2015;5:7055-62. DOI
123. Li W, Wang Q, Xu J, et al. Probing the surface of γ-Al_2O_3 by oxygen-17 dynamic nuclear polarization enhanced solid-state NMR spectroscopy. *Phys Chem Chem Phys* 2018;20:17218-25. DOI PubMed
124. Blanc F, Sperrin L, Jefferson DA, Pawsey S, Rosay M, Grey CP. Dynamic nuclear polarization enhanced natural abundance ^{17}O spectroscopy. *J Am Chem Soc* 2013;135:2975-8. DOI PubMed
125. Perras FA, Boteju KC, Slowing II, Sadow AD, Pruski M. Direct ^{17}O dynamic nuclear polarization of single-site heterogeneous catalysts. *Chem Commun* 2018;54:3472-5. DOI PubMed
126. Perras FA, Kobayashi T, Pruski M. Natural Abundance ^{17}O DNP two-dimensional and surface-enhanced NMR spectroscopy. *J Am Chem Soc* 2015;137:8336-9. DOI PubMed
127. Giovine R, Trébosc J, Pourpoint F, Lafon O, Amoureux JP. Magnetization transfer from protons to quadrupolar nuclei in solid-state NMR using PRESTO or dipolar-mediated refocused INEPT methods. *J Magn Reson* 2019;299:109-23. DOI PubMed
128. Zhao X, Hoffbauer W, Schmedt auf der Günne J, Levitt MH. Heteronuclear polarization transfer by symmetry-based recoupling sequences in solid-state NMR. *Solid State Nucl Magn Reson* 2004;26:57-64. DOI PubMed
129. Perras FA, Kobayashi T, Pruski M. PRESTO polarization transfer to quadrupolar nuclei: implications for dynamic nuclear polarization. *Phys Chem Chem Phys* 2015;17:22616-22. DOI PubMed
130. Chen CH, Gaillard E, Mentink-Vigier F, et al. Direct ^{17}O isotopic labeling of oxides using mechanochemistry. *Inorg Chem* 2020;59:13050-66. DOI PubMed PMC

131. Nagashima H, Trébosc J, Kon Y, Sato K, Lafon O, Amoureux JP. Observation of low-γ quadrupolar nuclei by surface-enhanced NMR spectroscopy. *J Am Chem Soc* 2020;142:10659-72. DOI PubMed
132. Khan SU, Al-Shahry M, Ingler WB Jr. Efficient photochemical water splitting by a chemically modified n-TiO_2. *Science* 2002;297:2243-5. DOI PubMed
133. Kudo A, Miseki Y. Heterogeneous photocatalyst materials for water splitting. *Chem Soc Rev* 2009;38:253-78. DOI PubMed
134. Zou Z, Ye J, Sayama K, Arakawa H. Direct splitting of water under visible light irradiation with an oxide semiconductor photocatalyst. *Nature* 2001;414:625-7. DOI PubMed
135. Cortright RD, Davda RR, Dumesic JA. Hydrogen from catalytic reforming of biomass-derived hydrocarbons in liquid water. *Nature* 2002;418:964-7. DOI PubMed
136. Fu Q, Saltsburg H, Flytzani-Stephanopoulos M. Active nonmetallic Au and Pt species on ceria-based water-gas shift catalysts. *Science* 2003;301:935-8. DOI PubMed
137. Takata T, Jiang J, Sakata Y, et al. Photocatalytic water splitting with a quantum efficiency of almost unity. *Nature* 2020;581:411-4. DOI PubMed
138. Liu Z, Huang E, Orozco I, et al. Water-promoted interfacial pathways in methane oxidation to methanol on a CeO_2-Cu_2O catalyst. *Science* 2020;368:513-7. DOI PubMed
139. Saavedra J, Doan HA, Pursell CJ, Grabow LC, Chandler BD. The critical role of water at the gold-titania interface in catalytic CO oxidation. *Science* 2014;345:1599-602. DOI PubMed
140. Merte LR, Peng G, Bechstein R, et al. Water-mediated proton hopping on an iron oxide surface. *Science* 2012;336:889-93. DOI PubMed
141. Hussain H, Tocci G, Woolcot T, et al. Structure of a model TiO_2 photocatalytic interface. *Nat Mater* 2017;16:461-6. DOI PubMed
142. Björneholm O, Hansen MH, Hodgson A, et al. Water at interfaces. *Chem Rev* 2016;116:7698-726. DOI PubMed
143. Lin L, Hisatomi T, Chen S, Takata T, Domen K. Visible-light-driven photocatalytic water splitting: recent progress and challenges. *Trends Chem* 2020;2:813-24. DOI
144. Wang ZT, Wang YG, Mu R, et al. Probing equilibrium of molecular and deprotonated water on TiO_2(110). *Proc Natl Acad Sci U S A* 2017;114:1801-5. DOI PubMed PMC
145. Du Y, Deskins NA, Zhang Z, Dohnálek Z, Dupuis M, Lyubinetsky I. Two pathways for water interaction with oxygen adatoms on TiO_2(110). *Phys Rev Lett* 2009;102:096102. DOI PubMed
146. Kristoffersen HH, Hansen JO, Martinez U, et al. Role of steps in the dissociative adsorption of water on rutile TiO_2(110). *Phys Rev Lett* 2013;110:146101. DOI PubMed
147. Kamal C, Stenberg N, Walle LE, et al. Core-level binding energy reveals hydrogen bonding configurations of water adsorbed on **TiO 2(110)** surface. *Phys Rev Lett* 2021;126:016102. DOI PubMed
148. Vittadini A, Selloni A, Rotzinger FP, Grätzel M. Structure and energetics of water adsorbed at TiO_2 anatase **101** and **001** surfaces. *Phys Rev Lett* 1998;81:2954-7. DOI
149. Tilocca A, Selloni A. Vertical and lateral order in adsorbed water layers on anatase TiO_2(101). *Langmuir* 2004;20:8379-84. DOI PubMed
150. Walle LE, Borg A, Johansson EMJ, et al. Mixed dissociative and molecular water adsorption on anatase TiO_2 (101). *J Phys Chem C* 2011;115:9545-50. DOI
151. Patrick CE, Giustino F. Structure of a water monolayer on the anatase TiO_2(101) surface. *J Phys Chem C* 2018;122:11954-60. DOI
152. Fasulo F, Piccini G, Muñoz-garcía AB, Pavone M, Parrinello M. Dynamics of water dissociative adsorption on TiO_2 anatase (101) at monolayer coverage and below. *J Phys Chem C* 2022;126:15752-8. DOI
153. Boles MA, Ling D, Hyeon T, Talapin DV. The surface science of nanocrystals. *Nat Mater* 2016;15:141-53. DOI PubMed
154. Zhang X, Qin J, Xue Y, et al. Effect of aspect ratio and surface defects on the photocatalytic activity of ZnO nanorods. *Sci Rep* 2014;4:4596. DOI PubMed PMC
155. Mueller DN, Machala ML, Bluhm H, Chueh WC. Redox activity of surface oxygen anions in oxygen-deficient perovskite oxides during electrochemical reactions. *Nat Commun* 2015;6:6097. DOI PubMed
156. Llordés A, Wang Y, Fernandez-Martinez A, et al. Linear topology in amorphous metal oxide electrochromic networks obtained via low-temperature solution processing. *Nat Mater* 2016;15:1267-73. DOI PubMed
157. Zandi O, Hamann TW. Determination of photoelectrochemical water oxidation intermediates on haematite electrode surfaces using operando infrared spectroscopy. *Nat Chem* 2016;8:778-83. DOI PubMed
158. Feng N, Liu F, Huang M, et al. Unravelling the efficient photocatalytic activity of boron-induced Ti^{3+} species in the surface layer of TiO_2. *Sci Rep* 2016;6:34765. DOI PubMed PMC
159. Setvín M, Aschauer U, Scheiber P, et al. Reaction of O_2 with subsurface oxygen vacancies on TiO_2 anatase (101). *Science* 2013;341:988-91. DOI PubMed
160. Peng YK, Keeling B, Li Y, et al. Unravelling the key role of surface features behind facet-dependent photocatalysis of anatase TiO_2. *Chem Commun* 2019;55:4415-8. DOI PubMed
161. Peng YK, Ye L, Qu J, et al. Trimethylphosphine-assisted surface fingerprinting of metal oxide nanoparticle by ^{31}P solid-state NMR: a zinc oxide case study. *J Am Chem Soc* 2016;138:2225-34. DOI PubMed
162. Peng YK, Chou HL, Edman Tsang SC. Differentiating surface titanium chemical states of anatase TiO_2 functionalized with various groups. *Chem Sci* 2018;9:2493-500. DOI PubMed PMC

163. Peng Y, Fu Y, Zhang L, et al. Probe-molecule-assisted NMR spectroscopy: a comparison with photoluminescence and electron paramagnetic resonance spectroscopy as a characterization tool in facet-specific photocatalysis. *ChemCatChem* 2017;9:155-60. DOI
164. Peng YK, Hu Y, Chou HL, et al. Mapping surface-modified titania nanoparticles with implications for activity and facet control. *Nat Commun* 2017;8:675. DOI PubMed PMC
165. Zheng A, Liu SB, Deng F. ^{31}P NMR chemical shifts of phosphorus probes as reliable and practical acidity scales for solid and liquid catalysts. *Chem Rev* 2017;117:12475-531. DOI PubMed
166. Zheng A, Huang SJ, Liu SB, Deng F. Acid properties of solid acid catalysts characterized by solid-state ^{31}P NMR of adsorbed phosphorous probe molecules. *Phys Chem Chem Phys* 2011;13:14889-901. DOI PubMed
167. Yao Q, Zhang L, Huang D, et al. MAS NMR studies on the formation and structure of oxygen vacancy on the CeO_2 {110} surface under a reducing atmosphere. *J Phys Chem C* 2023;127:13021-33. DOI
168. Wu Y, Wang Y, Huang D, et al. Direct quantification of oxygen vacancy on the TiO_2 surface by ^{31}P solid-state NMR. *Chem Catal* 2023;3:100556. DOI
169. Chu Y, Yu Z, Zheng A, et al. Acidic strengths of Brønsted and lewis acid sites in solid acids scaled by ^{31}P NMR chemical shifts of adsorbed trimethylphosphine. *J Phys Chem C* 2011;115:7660-7. DOI
170. Hu Y, Guo B, Fu Y, et al. Facet-dependent acidic and catalytic properties of sulfated titania solid superacids. *Chem Commun* 2015;51:14219-22. DOI PubMed
171. Zhang H, Yu H, Zheng A, Li S, Shen W, Deng F. Reactivity enhancement of 2-propanol photocatalysis on SO_4^{2-}/TiO_2: insights from solid-state NMR spectroscopy. *Environ Sci Technol* 2008;42:5316-21. DOI PubMed
172. Choi W, Termin A, Hoffmann MR. The role of metal ion dopants in quantum-sized TiO_2: correlation between photoreactivity and charge carrier recombination dynamics. *J Phys Chem* 1994;98:13669-79. DOI
173. Vamathevan V, Amal R, Beydoun D, Low G, Mcevoy S. Photocatalytic oxidation of organics in water using pure and silver-modified titanium dioxide particles. *J Photoch Photobio A* 2002;148:233-45. DOI
174. He C, Yu Y, Hu X, Larbot A. Influence of silver doping on the photocatalytic activity of titania films. *Appl Surf Sci* 2002;200:239-47. DOI
175. Jaegers NR, Wang Y, Hu JZ, Wachs IE. Impact of hydration on supported V_2O_5/TiO_2 catalysts as explored by magnetic resonance spectroscopy. *J Phys Chem C* 2021;125:16766-75. DOI
176. Stebbins JF. Aluminum substitution in rutile titanium dioxide: new constraints from high-resolution ^{27}Al NMR. *Chem Mater* 2007;19:1862-9. DOI
177. Chen X, Mao SS. Titanium dioxide nanomaterials: synthesis, properties, modifications, and applications. *Chem Rev* 2007;107:2891-959. DOI PubMed
178. Rumaiz AK, Woicik JC, Cockayne E, Lin HY, Jaffari GH, Shah SI. Oxygen vacancies in N doped anatase TiO_2: experiment and first-principles calculations. *Appl Phys Lett* 2009;95:262111. DOI
179. Cronemeyer DC. Infrared absorption of reduced rutile TiO_2 single crystals. *Phys Rev* 1959;113:1222-6. DOI
180. Tai Z, Sun G, Wang T, Li Z, Tai J. Netted C-doped TiO_2 mesoporous nanostructure decorated by Cu nanoparticles for photocatalytic CO_2 reduction. *ACS Appl Nano Mater* 2022;5:18070-9. DOI
181. Dong Y, Luo X, Wang Y, et al. A robust novel 0D/2D MoS_3 QDs/C-doped atomically thin TiO_2(B) nanosheet composite for highly efficient photocatalytic H_2 evolution. *Appl Surf Sci* 2022;599:153972. DOI
182. Li Y, Ren Z, Gu M, Duan Y, Zhang W, Lv K. Synergistic effect of interstitial C doping and oxygen vacancies on the photoreactivity of TiO_2 nanofibers towards CO_2 reduction. *Appl Catal B Environ* 2022;317:121773. DOI
183. Shayegan Z, Haghighat F, Lee C. Carbon-doped TiO_2 film to enhance visible and UV light photocatalytic degradation of indoor environment volatile organic compounds. *J Environ Chem Eng* 2020;8:104162. DOI
184. Yang Y, Liu L, Qi Q, et al. A low-cost and stable Fe_2O_3/C-TiO_2 system design for highly efficient photocatalytic H_2 production from seawater. *Catal Commun* 2020;143:106047. DOI
185. Noorimotlagh Z, Kazeminezhad I, Jaafarzadeh N, Ahmadi M, Ramezani Z. Improved performance of immobilized TiO_2 under visible light for the commercial surfactant degradation: role of carbon doped TiO_2 and anatase/rutile ratio. *Catal Today* 2020;348:277-89. DOI
186. Lettmann C, Hildenbrand K, Kisch H, Macyk W, Maier WF. Visible light photodegradation of 4-chlorophenol with a coke-containing titanium dioxide photocatalyst. *Appl Catal B Environ* 2001;32:215-27. DOI
187. Ohno T, Tsubota T, Nishijima K, Miyamoto Z. Degradation of methylene blue on carbonate species-doped TiO_2 photocatalysts under visible light. *Chem Lett* 2004;33:750-1. DOI
188. Xu C, Killmeyer R, Gray ML, Khan SU. Photocatalytic effect of carbon-modified n-TiO_2 nanoparticles under visible light illumination. *Appl Catal B Environ* 2006;64:312-7. DOI
189. Xu C, Shaban YA, Ingler WB, Khan SU. Nanotube enhanced photoresponse of carbon modified (CM)-n-TiO_2 for efficient water splitting. *Sol Energy Mater Sol Cells* 2007;91:938-43. DOI
190. Liu F, Feng N, Yang L, Wang Q, Xu J, Deng F. Enhanced photocatalytic performance of carbon-coated TiO_{2-x} with surface-active carbon species. *J Phys Chem C* 2018;122:10948-55. DOI
191. Chen C, Long M, Zeng H, et al. Preparation, characterization and visible-light activity of carbon modified TiO_2 with two kinds of carbonaceous species. *J Mol Catal A Chem* 2009;314:35-41. DOI
192. Rockafellow EM, Fang X, Trewyn BG, Schmidt-rohr K, Jenks WS. Solid-state ^{13}C NMR characterization of carbon-modified TiO_2.

Chem Mater 2009;21:1187-97. DOI

193. Feng N, Lin H, Deng F, Ye J. Interfacial-bonding Ti–N–C boosts efficient photocatalytic H_2 evolution in close coupling g-C_3N_4/TiO_2. *J Phys Chem C* 2021;125:12012-8. DOI
194. Feng G, Mao J, Sun T, et al. Nitrogen-doped titanium dioxide for selective photocatalytic oxidation of methane to oxygenates. *ACS Appl Mater Interfaces* 2024;16:4600-5. DOI PubMed
195. Bhowmick S, Saini CP, Santra B, et al. Modulation of the work function of TiO_2 nanotubes by nitrogen doping: implications for the photocatalytic degradation of dyes. *ACS Appl Nano Mater* 2023;6:50-60. DOI
196. Chen C, Wu M, Yang C, et al. Electron-donating N^-–Ti^{3+}–O_v interfacial sites with high selectivity for the oxidation of primary C–H bonds. *Cell Rep Phys Sci* 2022;3:100936. DOI
197. Kwon J, Choi K, Schreck M, Liu T, Tervoort E, Niederberger M. Gas-phase nitrogen doping of monolithic TiO_2 nanoparticle-based aerogels for efficient visible light-driven photocatalytic H_2 production. *ACS Appl Mater Interfaces* 2021;13:53691-701. DOI PubMed
198. Liang M, Bai X, Yu F, Ma J. A confinement strategy to in-situ prepare a peanut-like N-doped, C-wrapped TiO_2 electrode with an enhanced desalination capacity and rate for capacitive deionization. *Nano Res* 2021;14:684-91. DOI
199. Kong X, Peng Z, Jiang R, et al. Nanolayered heterostructures of N-doped TiO_2 and N-doped carbon for hydrogen evolution. *ACS Appl Nano Mater* 2020;3:1373-81. DOI
200. Reyes-garcia EA, Sun Y, Reyes-gil K, Raftery D. ^{15}N solid state NMR and EPR characterization of N-doped TiO_2 photocatalysts. *J Phys Chem C* 2007;111:2738-48. DOI
201. Feng N, Zheng A, Wang Q, et al. Boron environments in B-doped and (B, N)-codoped TiO_2 photocatalysts: a combined solid-state NMR and theoretical calculation study. *J Phys Chem C* 2011;115:2709-19. DOI
202. Feng N, Wang Q, Zheng A, et al. Understanding the high photocatalytic activity of (B, Ag)-codoped TiO_2 under solar-light irradiation with XPS, solid-state NMR, and DFT calculations. *J Am Chem Soc* 2013;135:1607-16. DOI PubMed
203. Zhao W, Ma W, Chen C, Zhao J, Shuai Z. Efficient degradation of toxic organic pollutants with Ni_2O_3/$TiO_{2-x}B_x$ under visible irradiation. *J Am Chem Soc* 2004;126:4782-3. DOI PubMed
204. Reyes-garcia EA, Sun Y, Raftery D. Solid-state characterization of the nuclear and electronic environments in a boron−fluoride co-doped TiO_2 visible-light photocatalyst. *J Phys Chem C* 2007;111:17146-54. DOI
205. Wu T, Xie Y, Yin L, Liu G, Cheng H. Switching photocatalytic H_2 and O_2 generation preferences of rutile TiO_2 microspheres with dominant reactive facets by boron doping. *J Phys Chem C* 2015;119:84-9. DOI
206. Liu G, Zhao Y, Sun C, Li F, Lu GQ, Cheng HM. Synergistic effects of B/N doping on the visible-light photocatalytic activity of mesoporous TiO_2. *Angew Chem Int Ed Engl* 2008;47:4516-20. DOI PubMed
207. Gopal NO, Lo HH, Ke SC. Chemical state and environment of boron dopant in B,N-codoped anatase TiO_2 nanoparticles: an avenue for probing diamagnetic dopants in TiO_2 by electron paramagnetic resonance spectroscopy. *J Am Chem Soc* 2008;130:2760-1. DOI PubMed
208. In S, Orlov A, Berg R, et al. Effective visible light-activated B-doped and B,N-codoped TiO_2 photocatalysts. *J Am Chem Soc* 2007;129:13790-1. DOI PubMed
209. Zaleska A, Sobczak JW, Grabowska E, Hupka J. Preparation and photocatalytic activity of boron-modified TiO_2 under UV and visible light. *Appl Catal B Environ* 2008;78:92-100. DOI
210. Coudurier G. Properties of boron-substituted ZSM-5 and ZSM-11 zeolites. *J Catal* 1987;108:1-14. DOI
211. Ruiter R, Kentgens A, Grootendorst J, Jansen J, van Bekkum H. Calcination and deboronation of [B]-MFI single crystals. *Zeolites* 1993;13:128-38. DOI
212. Dorn RW, Heintz PM, Hung I, et al. Atomic-level structure of mesoporous hexagonal boron nitride determined by high-resolution solid-state multinuclear magnetic resonance spectroscopy and density functional theory calculations. *Chem Mater* 2022;34:1649-65. DOI
213. Mark LO, Dorn RW, Mcdermott WP, et al. Highly selective carbon-supported boron for oxidative dehydrogenation of propane. *ChemCatChem* 2021;13:3611-8. DOI
214. Medek A, Harwood JS, Frydman L. Multiple-quantum magic-angle spinning NMR: a new method for the study of quadrupolar nuclei in solids. *J Am Chem Soc* 1995;117:12779-87. DOI
215. Wang SH, Xu Z, Baltisberger JH, Bull LM, Stebbins JF, Pines A. Multiple-quantum magic-angle spinning and dynamic-angle spinning NMR spectroscopy of quadrupolar nuclei. *Solid State Nucl Magn Reson* 1997;8:1-16. DOI PubMed
216. Smith M. Recent advances in experimental solid state NMR methodology for half-integer spin quadrupolar nuclei. *Prog Nucl Mag Res Sp* 1999;34:159-201. DOI
217. Dorn RW, Cendejas MC, Chen K, et al. Structure determination of boron-based oxidative dehydrogenation heterogeneous catalysts with ultra-high field 35.2 T ^{11}B solid-state NMR spectroscopy. *ACS Catal* 2020;10:13852-66. DOI PubMed PMC
218. Sasaki J, Peterson N, Hoshino K. Tracer impurity diffusion in single-crystal rutile (TiO_{2-x}). *J Phys Chem Solids* 1985;46:1267-83. DOI
219. Bak T, Burg T, Kang S, et al. Charge transport in polycrystalline titanium dioxide☆. *J Phys Chem Solids* 2003;64:1089-95. DOI
220. Gesenhues U. Al-doped TiO_2 pigments: influence of doping on the photocatalytic degradation of alkyd resins. *J Photoch Photobio A* 2001;139:243-51. DOI
221. Kotzamanidi S, Frontistis Z, Binas V, Kiriakidis G, Mantzavinos D. Solar photocatalytic degradation of propyl paraben in Al-doped

TiO_2 suspensions. *Catal Today* 2018;313:148-54. DOI

222. Murashkina AA, Rudakova AV, Ryabchuk VK, et al. Influence of the dopant concentration on the photoelectrochemical behavior of Al-doped TiO_2. *J Phys Chem C* 2018;122:7975-81. DOI
223. Gionco C, Livraghi S, Maurelli S, et al. Al- and Ga-doped TiO_2, ZrO_2, and HfO_2: the nature of O 2p trapped holes from a combined electron paramagnetic resonance (EPR) and density functional theory (DFT) study. *Chem Mater* 2015;27:3936-45. DOI
224. Su CY, Wang LC, Liu WS, Wang CC, Perng TP. Photocatalysis and hydrogen evolution of Al- and Zn-doped TiO_2 nanotubes fabricated by atomic layer deposition. *ACS Appl Mater Interfaces* 2018;10:33287-95. DOI PubMed
225. Yang L, Feng N, Deng F. Aluminum-doped TiO_2 with dominant {001} facets: microstructure and property evolution and photocatalytic activity. *J Phys Chem C* 2022;126:5555-63. DOI
226. Xu J, Wang Q, Li S, Deng F. Solid-state NMR in zeolite catalysis. 1st edition. Singapore: Springer. 2019. DOI
227. Qi G, Wang Q, Xu J, Deng F. Solid-state NMR studies of internuclear correlations for characterizing catalytic materials. *Chem Soc Rev* 2021;50:8382-99. DOI PubMed